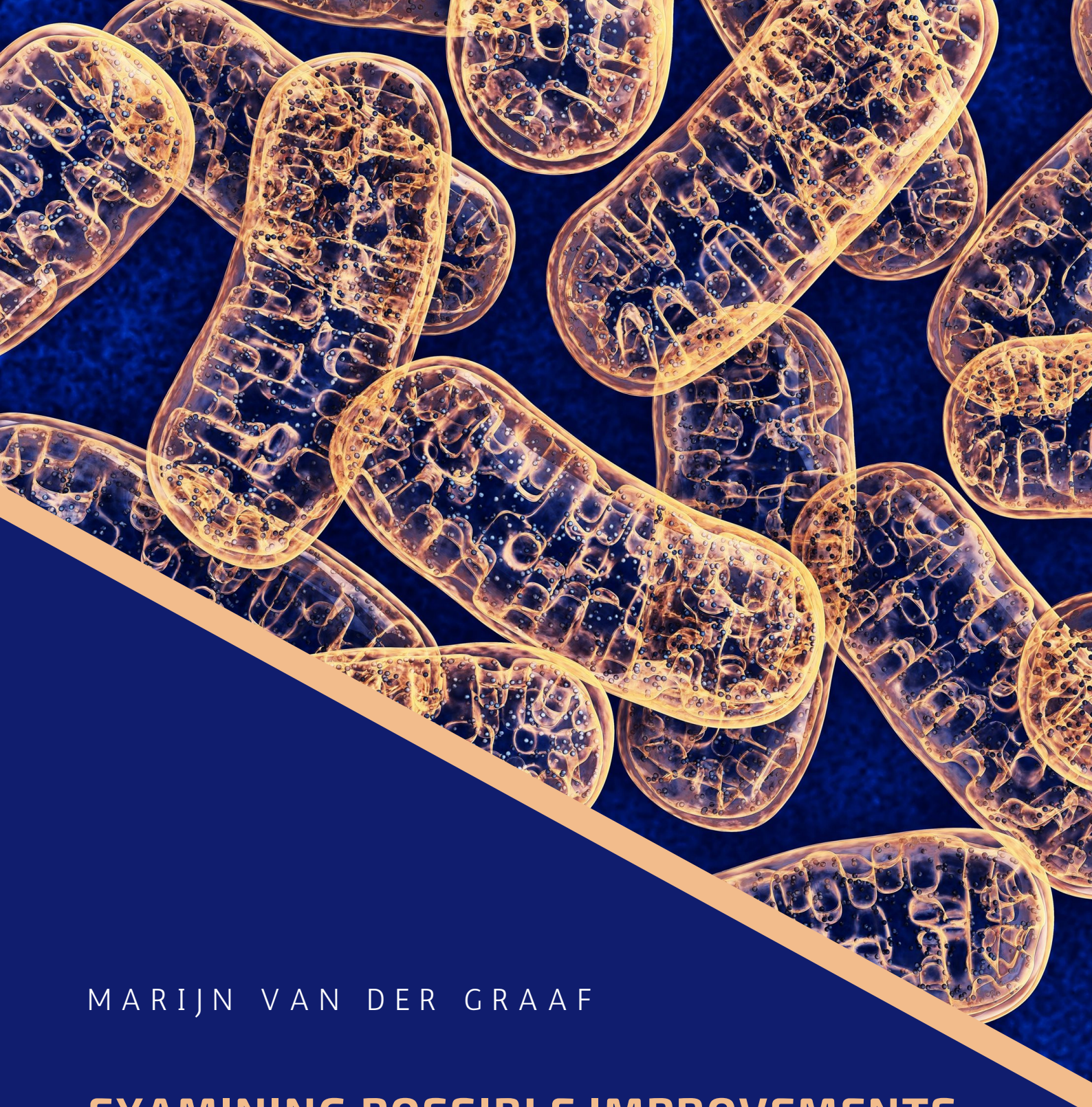

MARIJN VAN DER GRAAF

EXAMINING POSSIBLE IMPROVEMENTS TO NON-INVASIVELY MEASURE MITOCHONDRIAL OXYGEN TENSION IN A CLINICAL DEVICE

MASTER THESIS TECHNICAL MEDICINE
DECEMBER 2022

Examining Possible Improvements to Non-Invasively Measure Mitochondrial Oxygen Tension in a Clinical Device

Marijn van der Graaf

Student number: 4468708

21 December 2022

Thesis in partial fulfilment of the requirements for the joint degree of Master of Science in

Technical Medicine

Leiden University ; Delft University of Technology ; Erasmus University Rotterdam

Master thesis project (TM30004 ; 35 ECTS)

Dept. of Anesthesiology, Erasmus MC

May 2022 – December 2022

Supervisor(s):

Dr. Bert Mik

Dr. Floor Harms

Thesis committee members:

Dr. John van den Dobbelsteen, TU Delft (chair)

Dr. Bert Mik, Erasmus MC

Dr. Floor Harms, Erasmus MC

Universiteit Leiden

TU Delft Delft University of Technology

Erasmus Universiteit Rotterdam

Examining Possible Improvements to Non-Invasively Measure Mitochondrial Oxygen Tension in a Clinical Device

M.E. (Marijn) van der Graaf, MSc student Technical Medicine
Educational program Technical Medicine; Leiden University Medical Center, Delft University of Technology & Erasmus University Medical Center Rotterdam

Abstract

Background and objectives: Mitochondria require oxygen to generate energy for essential cellular processes. An in-vivo non-invasive technique to monitor mitochondrial oxygen tension ($mitoPO_2$) is the protoporphyrin IX-triplet state lifetime technique. Protoporphyrin IX (PpIX), one of the key components of heme, is naturally present in the mitochondria. Topical administration of 5-aminolevulinic acid hydrochloride (ALA) increases PpIX concentration in the skin. After excitation with a laser pulse, PpIX emits red light with an oxygen-dependent delayed fluorescence lifetime. This signal is detected by a photomultiplier and the $mitoPO_2$ can be derived from this. A clinical device has been developed using this technique. Although this device has been proven feasible, improvements in reliability and practicality are needed. This work aims to investigate possible improvements to the components of this device for better application in a clinical setting. The main areas of improvement are the excitation wavelength, the detection of the signal, and the light source.
Excitation wavelength: First, wavelengths from 415 nm to 695 nm are explored as possible excitation wavelengths. Second, four excitation wavelengths that exhibit low noise are investigated in more detail. For a better comparison, the pulse energy per wavelength is equated. The excitation wavelengths 415 nm and 515 nm showed low noise, no oversaturation, and accurate fits. These two excitation wavelengths are then validated on three test subjects with skin types II, IV, and V on the Fitzpatrick scale. Oxygen-dependent lifetimes are obtained in all test subjects with an excitation wavelength of 415 nm.
Detection: A new detector is explored to replace the large and expensive photomultiplier. The detector is tested in a fluorescent solution and on human skin. The first experiments resulted in oversaturation of the detector. To prevent this, several combinations of band-pass, long-pass, and absorption filters are tested. Even with these filters, the detector was oversaturated by the light pulse from the laser.
Light source: Two light sources are investigated as possible replacements for the currently used laser. These were first tested in a 10 µM PpIX solution. No delayed fluorescence was observed because the light sources and detector could not be placed close enough to each other. Therefore, for the measurements in human skin, the light source was coupled into a fiber. Both light sources showed oxygen-dependent lifetimes, suggesting that they are suitable for this application. As a final step, related parameters were optimized to reduce oversaturation and noise. These are described in the Confidential Appendix.
Conclusion: The potential of 415 nm as an excitation wavelength is demonstrated, but these results should be validated in more test subjects. The light sources showed the potential to replace the current laser, which could reduce maintenance and increase reliability. The next step should be to combine the 415 nm excitation wavelength, light source, and detector into a prototype to explore their combined potential.

1. INTRODUCTION

Humans need oxygen to survive.[1] Oxygen is inhaled, exchanged to the blood, and transported via the arteries and capillaries to the cells. The majority of this oxygen is used in the mitochondria in the cells during oxidative phosphorylation. This is a process to efficiently generate adenosine triphosphate (ATP), the energy source of the cell.[2–4] Without oxygen in the mitochondria, anaerobic metabolism would take place. This anaerobic metabolism produces less ATP. When not enough ATP is produced, it affects almost all cellular processes and can ultimately lead to cell death.[5–7]

Monitoring the local oxygen supply to the tissues can help to intervene in time when oxygen deficiency threatens. There are various non-invasive techniques to monitor tissue oxygenation. A recent development is the protoporphyrin IX-triplet state lifetime technique (PpIX-TSLT), which allows non-invasive in vivo measurement of mitochondrial oxygen tension.[5]

1.1 Theory of PpIX-TSLT

Protoporphyrin IX (PpIX) is an organic structure and is one of the key components of hemoglobin. It is synthesized inside the mitochondria. When PpIX is excited with light, it absorbs a photon and changes from the ground state to the excited singlet state. The excited PpIX releases a photon and goes back to the ground state in a specified time, called a lifetime. The excited singlet state can shift to the excited triplet state, due to intersystem crossing. Oxygen is also

present in the mitochondria and has a triplet state as ground state, something very unusual.[8] If the oxygen and the excited PpIX collide, the energy from the PpIX triplet state transfers to the triplet ground state of oxygen. When more oxygen is present, these collisions will occur more frequently, resulting in a short lifetime of PpIX.[9] The different energy states of PpIX and oxygen are shown in Figure 1, as described by Mik *et al.*[9]

PpIX lifetimes can be obtained using for instance phosphorescence, prompt fluorescence, and delayed fluorescence. When the energy of the excited singlet state shifts to the excited triplet state before the photon is released, this is called phosphorescence. In fluorescence, a photon is released after relaxation of PpIX from the singlet state to the ground state. For delayed fluorescence, bidirectional intersystem crossing occurs between the excited singlet state and the excited triplet state. Due to this extra step, the fluorescence is delayed compared to prompt fluorescence and thereby suitable to measure the lifetimes in this application. The emission spectra for prompt and delayed fluorescence are equal but differ in intensity.[9] The state transitions in phosphorescence and delayed fluorescence are shown in Figure 1.

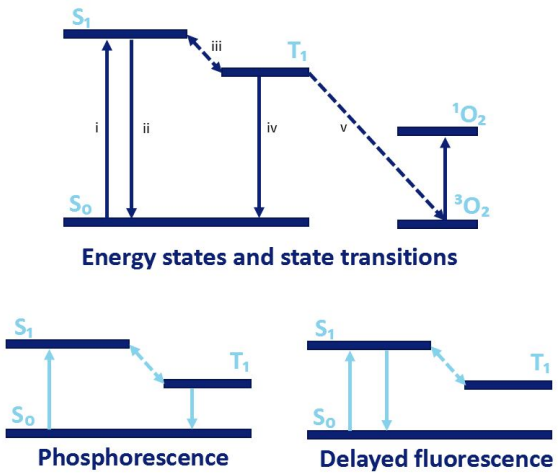

Figure 1: Energy states and state transitions of protoporphyrin IX and oxygen, adjusted from Mik et al.[9] i: absorption; ii: fluorescence; iii: intersystem crossing; iv: phosphorescence; v: energy transfer; S_0 and S_1 are the ground state and first excited singlet states of PpIX, T_1 is the first excited triplet state of PpIX and $^3O_2$ and $^1O_2$ are the triplet ground state and excited singlet oxygen, respectively.

The natural concentration of PpIX in mitochondria is too low to detect with the PpIX-TSLT, therefore 5-aminolevulinic acid hydrochloride (ALA) is locally applied to enhance PpIX concentrations via a cascade of cell processes. Sufficient detection of PpIX is possible after approximately 3 hours.[5,10]

Thus, delayed fluorescence is measured when PpIX shifts from the excited singlet state to the ground state after bidirectional intersystem crossing to the triplet state, hereby releasing a photon. As a result, emitted light with a wavelength of 630 to 700 nm is produced.[5,9] A high oxygen tension inside the mitochondria results in a short lifetime of PpIX since more oxygen collides with PpIX. These principles are described by Mik *et al.* and are visualized in Figure 2.[9]

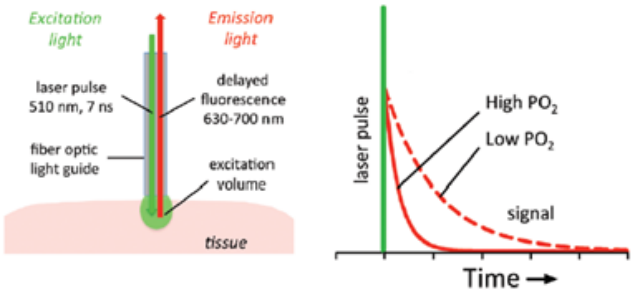

(a) *(b)*

Figure 2: The basic principles of mitochondrial oxygen tension ($mitoPO_2$) measurements. (a) Schematic overview of the measurement and (b) the emitted delayed fluorescence is oxygen-dependent. Adjusted from Mik et al.[9]

The delayed fluorescence signal is used to calculate the lifetime and corresponding $mitoPO_2$. A rectangular fit is used to approximate the data points of the delayed fluorescence signal:[9]

$$Y_R(t) = exp\left(-\left(\frac{1}{\tau_0} + k_q PO_2\right)t\right)\frac{sinh\,(k_q \delta t)}{k_q \delta t}$$

in which $Y_R(t)$ is the estimated rectangular fit, τ_0 is the lifetime at zero oxygen, k_q is the quenching constant, and δ is half the width of the rectangular distribution.

From the coefficients of this rectangular fit, the lifetime is determined. This lifetime can then be used to calculate the mitochondrial oxygen tension ($mitoPO_2$):[9]

$$mitoPO_2 = \frac{\frac{1}{\tau} - \frac{1}{\tau_0}}{k_q}$$

with τ as the delayed fluorescence lifetime, τ_0 as the lifetime at zero oxygen and k_q as the quenching constant.

1.2 Previous research

In the last 2 decades, PpIX-TSLT has been further developed and researched. This led to the development of a device called the COMET, an acronym for Cellular Oxygen METabolism, to measure $mitoPO_2$ using PpIX-TSLT. The COMET is shown in Figure 3. The COMET comprises a rigid cable, including a fiber, to the skin probe. A Q-Switched laser with a wavelength of 515 nm is used to excite PpIX. A Q-Switched laser can produce a pulsed laser beam with high peak power.[11] A red-sensitive photomultiplier

detects the delayed fluorescence signal, from which the mitoPO$_2$ is subsequently calculated.[12]

(a) COMET device *(b) COMET fiber and probe*

Figure 3: COMET as described by Ubbink et al.[12]

Experiments have been performed on isolated liver cells, isolated livers, and in vivo rat livers.[13] After the method was shown to be feasible, the PpIX-TSLT was also tested on other organs under various conditions, e.g. the heart and the skin of rats and pigs.[10,14–16] It was found that measurements on the skin can serve as an early indicator to limit hemodilution, and therefore function as a possible trigger for blood transfusion.[17,18]

In 2016, the first study in healthy volunteers was successfully performed.[19] Subsequently, multiple in-human studies were performed, researching the mitoPO$_2$ in various conditions, diseases, and patient groups.[20–24] MitoPO$_2$ is measured in millimeters of mercury (mmHg), a frequently used unit for pressure in medicine. 1 mmHg corresponds with 1 Torr or 133.322 Pa.[25] The measurements are performed on the skin at the sternum or upper arm. The cutaneous mitoPO$_2$ has been shown to be capable of reflecting the mitochondrial parameters of other vital organs.[17,26] An overview of published studies regarding PpIX-TSLT is given in Appendix Figure 23.

1.3 My experiences with the COMET

During my internship I performed some clinical COMET measurements myself. In my experience, the user interface of the device is informative and intuitive. Data are displayed clearly and changes in mitoPO$_2$ and signal quality over time are easy to see. The COMET was used during surgery and postoperatively. The COMET should be placed well away from the patient in the operating room so that the anesthesiologists and surgeons have room to work. A longer cable, in my perspective, would make it easier to position the COMET so that it would not be in the way. Postoperatively, there was enough space to position the COMET close to the patient. Also, the cable cannot be bent or dropped because it contains a sensitive fiber, that would otherwise break. This is very impractical in the operating room. The laser is vulnerable as well. Laser failures occurred several times, sometimes fixed after a few minutes, but sometimes requiring repair.

Despite these practical problems, I think the mitoPO$_2$ measurements are of additional value in the clinic. This physiological parameter reflects the current oxygen tension in the mitochondria at any given time. Clinically, arterial lactate levels are used to assess oxygenation. However, lactate is a derived parameter, elevations can have various causes, and blood draws are invasive procedures. In addition, lactate measurements are not performed at the rate that the COMET can perform measurements.

1.4 Research goal

The goal of this research is to investigate possible improvements for the COMET, focusing on the reliability and practicality of the device. To reach this goal, the project is divided in three subprojects; the excitation wavelength, the detection side, and the light source.

1.5 Excitation wavelength

An excitation wavelength of 515 nm (green light) was chosen during the development of this technique. Figure 4 shows the absorption spectrum of protoporphyrin IX, as reported by Falk *et al.*[27] An absorption spectrum reflects the intensity of absorbed energy per wavelength. The absorption spectrum of PpIX shows the highest peak at 400 nm (violet light), and much smaller peaks at 515, 540, 570, and 630 nm. This means that the energy is absorbed approximately ten times better using a wavelength of 400 nm. However, the second highest peak at 515 nm is chosen as the excitation wavelength, because longer wavelengths penetrate deeper into the skin. Green light penetrates deeper into the skin than violet light. This difference in penetration depth could affect the measurements. However, there is no consensus on the exact penetration depth of the different wavelengths.[28,29] Wavelengths other than 515 nm have never been tested before for this application. Despite the fact that different wavelengths penetrate to different depths, we do not know which excitation wavelengths will result in accurate measurements. Therefore, a wavelength study is performed to determine which wavelengths in the range of 415 to 695 nm can be used for PpIX-TsLT measurements.

With varying excitation wavelengths to test, another question arises; does skin type influence photon penetration in this application? People with darker skin color have more melanin, a strong light-absorbing pigment. Therefore, when light is excited, more photons are absorbed by melanin, and fewer photons pass through this layer.[30] This could potentially result in fewer photons reaching the mitochondria, complicating

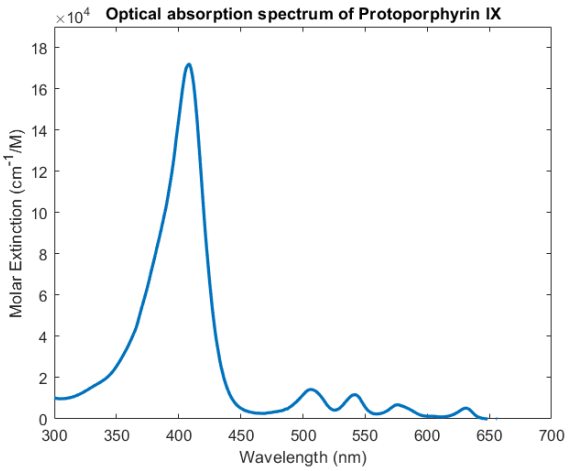

Figure 4: The absorption spectrum of protoporphyrin IX reported by Falk et al.[27]

the PpIX-TSLT technique and leading to inadequate measurements. Therefore, all kinds of skin types should be taken into account when exploring other excitation wavelengths.

1.6 Detection

The COMET detects and accumulates the delayed fluorescence signal with a red-sensitive photomultiplier.[12] This photomultiplier is reliable but relatively large and expensive. Nowadays, there are many multiplier systems, with different reliability, size, and cost. We investigate the possibilities of a new detector and its potential to replace the photomultiplier. This new detector will be referred to as 'detector A' in this paper. Specifications for this detector can be found in the Confidential Appendix.

1.7 Light source

In addition to possible improvements in excitation wavelength and detection of the signal, the potential of a new light source is also being investigated. Currently, a laser is used that is relatively large and has high safety requirements, resulting in a rigid cable around the fiber. In addition, the cost of the current laser is relatively high compared to other existing light sources. In recent years, there has been tremendous development in this field, leading to many possibilities for light sources with different powers, pulse widths, and prices. In this part of the project, the possibilities of other types of light sources are explored, which are referred to as 'light source A' and 'light source B' in this paper. Specifications for these light sources can be found in the Confidential Appendix. Light sources A and B will be investigated for their emitted light pulse and feasibility to measure on ALA-prepared human skin.

2. METHODS

2.1 Excitation wavelength

The excitation wavelength subproject consists of three experiments. First, wavelengths ranging from 415 nm to 695 nm, with steps of 20 nm are studied. Then, the wavelengths that show little to no noise are further analyzed. The pulse energy per wavelength is equated, and measurements are performed with equal pulse energy for each wavelength. Finally, the wavelengths and corresponding pulse energies are validated in different skin types.

The same setup is used for all three experiments. The Opolette 355 tunable laser with a frequency of 10 Hz excites light with varying wavelengths, ranging from 415 to 695 nm. Accessory Opotek software is used to control the laser. A prototype probe (no. 4) from Photonics Healthcare is used to guide the laser pulse to the skin and to forward the emitted light to the photomultipliers. Two photomultipliers (Hamamatsu H11526-20-NF) are used for the detection of the 635 nm and 660 nm emitted light, with the possibility to vary the gain and the delay time. The second photomultiplier with a detection wavelength of 660 nm is added to visualize potential second-order kinetics of PpIX. The setup of the photomultipliers including serial numbers is shown in Figure 5. Two power supplies provide the photomultipliers with a voltage of +5/0/-5 V and +/- 15 V, respectively. A pulse generator is used to gate the photomultipliers to prevent oversaturation. A data acquisition system (National Instruments USB-6356) is used, and is controlled using LabView. A schematic overview of this setup is shown in Figure 6. The captured signals are subsequently visualized and analyzed using MATLAB.

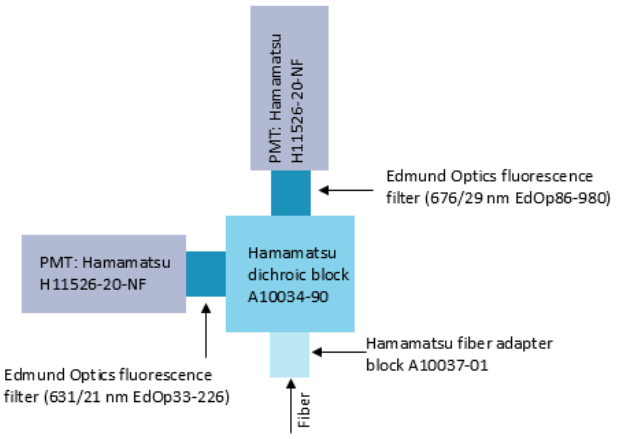

Figure 5: Schematic setup of photomultipliers

In the first experiment, a quick exploration of potential excitation wavelengths between 415 and 695 nm, with steps of 20 nm, is performed. The Q-Switch, one of the parameters to determine the pulse energy, of the Opolette is set at 180 µs.The photomultipliers increase

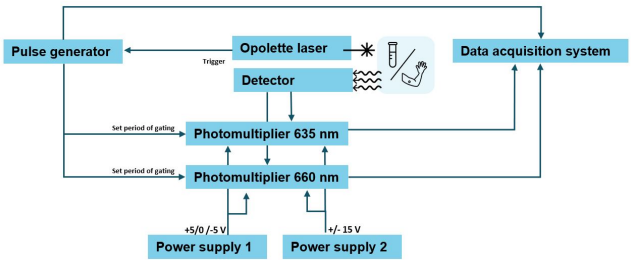

Figure 6: Schematic setup for the excitation wavelength subproject

the signal with a gain of 2×10^6 and a gating delay of ± 5 µs. The experiments are performed on the right upper arm, after application of an ALA-adhesive >10 hours before. Ambient light is minimized. The optimal laser power is found using attenuation filters to avoid saturation but ensure sufficient signal to minimize noise. For each wavelength, three measurements are performed, to average and compare the measurements per wavelength. The signals are visualized in separate figures, and a rectangular fit is created to model the lifetime. When the signal is largely scattered or has a limited voltage range, the rectangular fit will be less accurate for the calculation of the mitoPO$_2$. The lifetimes and fits are then rated from 1 (inadequate) to 4 (satisfactory).

Next, the satisfactory excitation wavelengths from the first experiment are further explored. To ensure a fair comparison between the wavelengths, the excited light should contain the same pulse energy for every wavelength. The chosen wavelength, Q-Switch delay, and attenuation filters together determine the pulse energy. Combinations of these three aspects are constructed to achieve a pulse energy of 10, 20, 40, and 100 µJ, respectively. These settings are shown in Table 2 in the Appendix. The pulse energy is determined using a laser power meter connected to StarLab 3.80 software. Subsequently, measurements are performed in human skin for these four pulse energies at the promising wavelengths following from the first experiment. The photomultipliers increase the signal with a gain of 2×10^5 and a gating delay of ± 5 µs. ALA is applied to the forearm >10 hours prior.

To ensure the measured lifetimes represents the mitochondrial oxygen tension, it is important to examine if the signal is oxygen-dependent. This means that the lifetime is enlarged when less oxygen is present. In human skin measurements an inflated blood pressure band or pressure on the probe reduces the oxygen present inside the mitochondria - since the oxygen influx is minimized but at the same time the oxygen consumption is continued - and oxygen-dependency can easily be investigated.

For every wavelength and pulse energy, six measurements are performed. The first three measurements are in oxygenated condition, then the blood pressure band is inflated, and after at least 30 seconds, three measurements in absence of oxygen are performed. To test if the chosen excitation wavelength is sufficient, oxygen-dependency should be clearly seen, the signal should not saturate, the signal should not be largely scattered, and the rectangular fits should be representative for the measured data points.

Ultimately, in the third experiment, excitation wavelengths with corresponding pulse energies are tested in different skin types. According to the Fitzpatrick scale, skin types can be divided into six types, varying from type I (very light skin tone) to type VI (very dark skin tone).[31] Three test subjects with varying skin types contributed to this experiment. An ALA adhesive is applied at least 10 hours prior to the measurements and placed on the upper arm. The setup and settings are similar to the second experiment. Also, six measurements per wavelength are performed, three in normal oxygenated condition, and three in absence of oxygen. This lack of oxygen is generated by applying pressure on the skin with the probe. The data is visualized and the results from the different wavelengths and skin types are compared. Ultimately, we indicate which wavelengths with corresponding pulse energies show an oxygen-dependent lifetime for all examined skin types.

2.2 Detector

For the second subproject, a small circuit containing detector A is constructed, consisting of the Opolette 355 tunable laser, detector A with connected filters, a power supply, an oscilloscope, and a data acquisition system (National Instruments USB-6356. The tunable laser is set at a wavelength of 515 nm to excite PpIX in a solution or tissue. Detector A captures the emitted light, and is visualized by the oscilloscope and data acquisition system. LabView and Opotek software are used to control the data acquisition system and laser. This setup is visualized in Figure 7.

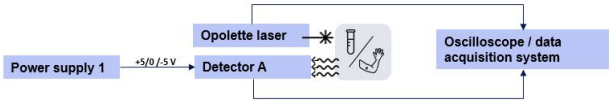

Figure 7: Schematic setup for the detector subproject

Also for this subproject, three experiments are performed. First, the characteristics of detector A are explored. Therefore, we position the laser fiber behind detector A to prevent the detector captures direct light. Ambient light is minimized to prevent oversaturation of the detector. A visualization is shown in Figure 16 in the Confidential Appendix.

Second, we experiment with (combinations of) band-pass, long-pass and absorptive filters to optimize the measured signals. The available filters are listed in Table 3 in the Appendix. An available fluorescent solution of palladium-meso-tetra(4-carbocyphenyl)-porphine (PdP) is used. The laser fiber is positioned a few millimeters above the PdP solution, and detector A is positioned beneath the solution, and a stabilizing ring is used. The Q-Switched laser excited light with a wavelength of 515 nm, a frequency of 5 Hz, and a Q-Switch of 210 µs. The setup is shown in Figure 17 in the Confidential Appendix.

Third, measurements are performed on human skin. Two detectors are covered with three band-pass filters each (635/20 nm and 660/40 nm, respectively) and one long-pass filter (>610 nm). The Opolette 355 tunable laser is set at 515 nm, a frequency of 20 Hz and a pulse energy of 10 µJ. The laser is connected to a fiber, which is situated between the detectors. The detectors and fiber are fixated on cardboard, as shown in Figure 18 in the Confidential Appendix. The ALA adhesive is applied >10 hours before the measurements. Then, measurements in skin with and without the ALA adhesive are performed. Oxygen-dependency is tested by applying local pressure.

The tiny delayed fluorescence lifetimes pale in comparison to the massive light pulse produced by the light source. This light source will probably arise problems regarding the detection of the delayed fluorescence lifetime. Consequently, a setup is constructed as described in the Confidential Appendix. Unfortunately, we did not have enough time to complete this configuration, and therefore we were unable to conduct the necessary tests.

2.3 Light source

In this subproject, possible replacements for the Q-Switched laser are explored. Multiple light sources with different powers and costs are purchased. Light source A and light source B, both with a power of 1 W, are analyzed. A light source driver is built in-house, enabling easy implementation of a light source. This driver is shown in Figure 19 in the Confidential Appendix. The setup consists of a pulse generator generating pulses of 0-5 V with varying frequencies and pulse widths, a power supply with an adjustable voltage based on the used light source, and an oscilloscope for visualization. The voltage applied to the light source driver depends on the current. We increase voltage step-wise until the current through the light sources reaches the threshold current to approach the maximal power of 1 Watt. To visualize the experimental setup, a schematic setup is shown in Figure 8. A detector is used to capture the emitted PpIX signal, and two photomultipliers (Hamamatsu H11526-20-NF) connected to two power supplies are used to accumulate the signal with an adjustable gain. The photomultipliers are also connected to the pulse generator, which enables adjustable gating to prevent oversaturation.

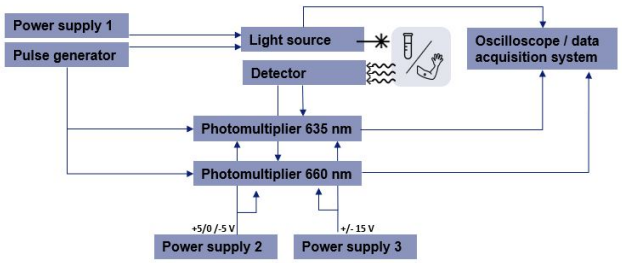

Figure 8: Schematic setup for the light source subproject

First, we test the possibilities to use light source A and light source B without being attached to a laser fiber. In the first experiment, we compare the PpIX lifetimes between a test tube containing a solution of 10 µM PpIX in dimethylformamide (DMF) and a test tube only containing DMF. The setup is shown Confidential Appendix Figure 20. The photomultipliers increase the signal with a gain of 2×10^6.[32] Varying positions of the detector probe relative to the light source are explored, to optimally capture the delayed fluorescence signal. Multiple positions are explored, for instance at different angles, perpendicular and above each other.

Then, measurements in human skin are performed. A fiber was essential for the measurements in human skin. Without the fiber, the light source and detector would have had to be placed very close to the skin and each other. This was not possible with the bulky prototypes we had. By coupling both the light source and the photomultipliers into the fiber, we can excite and detect the same area of the skin, which is necessary to detect a delayed fluorescence lifetime. This can be seen in Figure 21 in the Confidential Appendix. The skin is primed with ALA at least 3 hours before,[5,10] but preferably longer. Several settings are varied, these are described in the Confidential Appendix. An inflated blood pressure band or application of local pressure is used to examine oxygen-dependency. We examined if the excitation with light source A and light source B can result in an oxygen-dependent lifetime.

3. RESULTS

3.1 Excitation wavelength

In the first experiment of this subproject, excitation wavelengths between 415 and 695 nm are investigated. An ALA adhesive is applied to the upper arm ≥10 hours beforehand. The photomultiplier contains a 635 nm filter. A laser power of 100% oversaturated the results, as did the laser powers of 50% and 12.5%.

At a laser power of 6.25%, this oversaturation no longer occurred. Therefore, this laser power is used for the measurements. The lifetimes are visualized and rated from 1 (insufficient) to 4 (satisfactory), as shown in Table 1, along with a combined score per excitation wavelength and measured pulse energy. If the rectangular fit could not be created, N/A is noted. An example of a satisfactory and insufficient measurement can be found in Figure 9, measured with an excitation wavelength of 415 nm and 575 nm, respectively. An overview of all measurements performed can be found in Figures 24-37 in the Appendix. The wavelengths 415, 435, 495, 515, 535, and 635 nm are evaluated with 3/4 or 4/4 points. Lasers with excitation wavelengths of 435 and 495 nm are not widely available or excitation wavelengths close by showed similar or more promising results. These wavelengths are therefore not further considered. The wavelengths 415, 515, 535, and 635 nm remain candidates and are further investigated.

Table 1: Pulse energy and quality rating per excitation wavelength

λ (nm)	Pulse Energy (mean+std)	Round 1	Round 2	Round 3	Total
415	6.25±1.2 µJ	****	**	****	***
435	19.80±1.5 µJ	****	**	***	***
455	36.54±2.1 µJ	**	*	**	*
475	35.40±2.1 µJ	*	*	**	*
495	31.26±1.9 µJ	****	**	****	***
515	29.95±2.0 µJ	****	****	****	****
535	30.23±2.3 µJ	****	**	***	***
555	25.07±2.5 µJ	*	*	*	*
575	16.19±2.2 µJ	**	*	*	*
595	15.13±2.1 µJ	**	*	*	*
615	12.51±1.8 µJ	**	*	**	*
635	15.01±1.7 µJ	****	****	****	****
655	11.95±1.2 µJ	*	N/A	*	*
675	5.80±1.2 µJ	N/A	N/A	N/A	*
695	8.90±1.6 µJ	*	*	N/A	*

λ; Excitation wavelength in nanometers, std; standard deviation, N/A; not applicable

Second, these four possible excitation wavelengths are further optimized and compared. For every wavelength, attenuation filters and Q-Switch delays are combined to achieve pulse energies of 10, 20, 40 and 100 µJ. The Opolette laser is most stable using a low Q-Switch delay, (minimum of 145 µs), so attenuation filters are added to accomplish the required pulse energies using a low Q-Switch value. Visualizations of all performed measurements are shown in Appendix Figures 38-40. Due to high levels of noise or lack of oxygen-dependency, the wavelengths 530 nm and 635 nm are not suitable as excitation wavelengths in this application. For 635 nm, this is probably because the photomultiplier operates with a detection wavelength of 635 nm. Measurements using excitation wavelengths of 415 nm and 515 nm did show minor noise and were oxygen-dependent. For 415 nm, a pulse energy of 20-40 µJ presented the least noisy

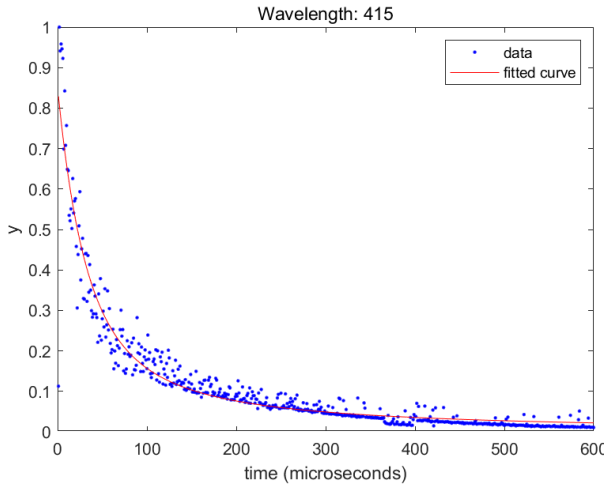

(a) Example of satisfactory rectangular fit

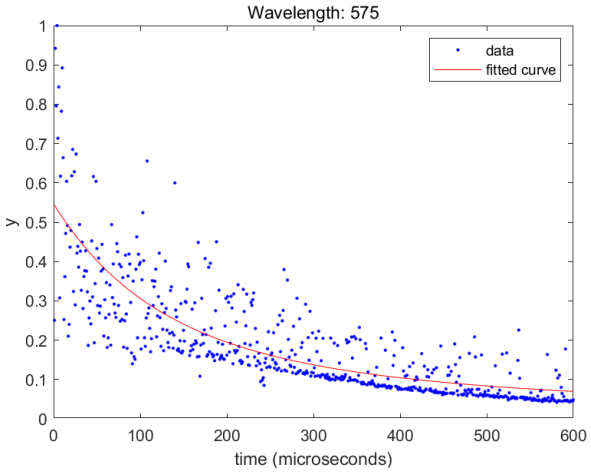

(b) Example of insufficient rectangular fit

Figure 9: Examples of satisfactory and insufficient rectangular fit measured at excitation wavelengths of 415 nm and 575 nm, respectively.

lifetimes and showed oxygen-dependency. This was 100 µJ for measurements with 515 nm. These results will be validated in test subjects with varying skin tones in the following experiment.

The third experiment included three test subjects with different skin tones (type II, IV, and V regarding the Fitzpatrick scale). ALA is administered at least 10 hours before the measurements. In Figure 10, measurements using an excitation wavelength of 415 nm and 515 nm are visualized for every test subject. All measurements can be found in Appendix Figures 41-43. For every test subject, an oxygen-dependent lifetime was found using an excitation wavelength of 415 nm. However, the maximal pulse energy at which no oversaturation occurs differed. At 415 nm, this was a pulse energy of 10 µJ for the test subjects with skin type II and IV, and 20 µJ for the test subject with skin type V. Measurements using 515 nm showed an oxygen-dependent lifetime for the test subjects of skin type II and IV using 100 µJ.

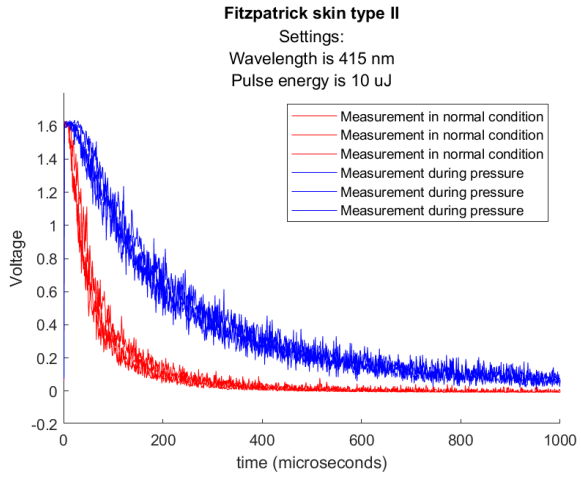

(a) Test subject with Fitzpatrick scale II
Excitation wavelength: 415 nm; pulse energy: 10 μJ

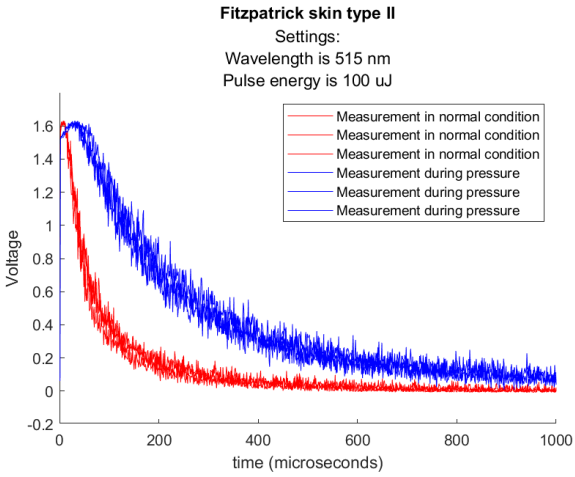

(b) Test subject with Fitzpatrick scale II
Excitation wavelength: 515 nm; pulse energy: 100 μJ

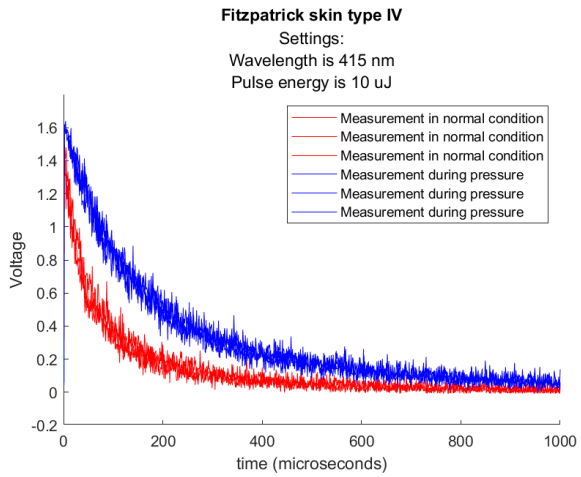

(c) Test subject with Fitzpatrick scale IV
Excitation wavelength: 415 nm; pulse energy: 10 μJ

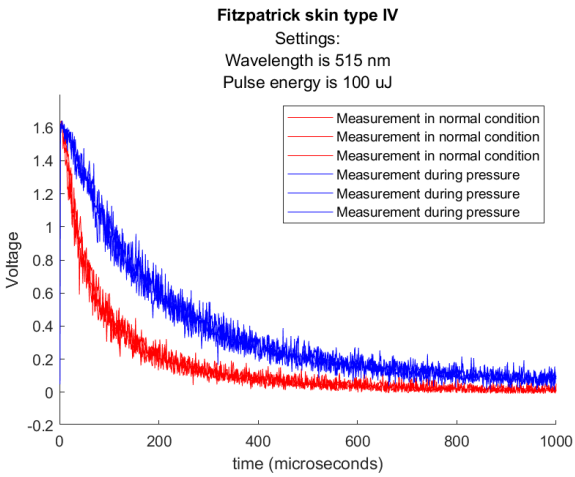

(d) Test subject with Fitzpatrick scale IV
Excitation wavelength: 515 nm; pulse energy: 100 μJ

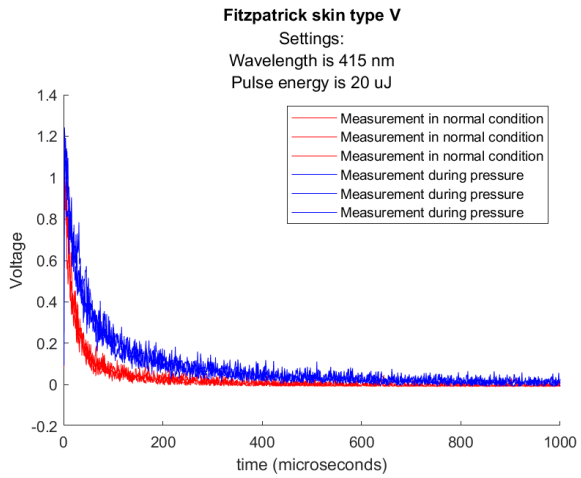

(e) Test subject with Fitzpatrick scale V
Excitation wavelength: 415 nm; pulse energy: 20 μJ

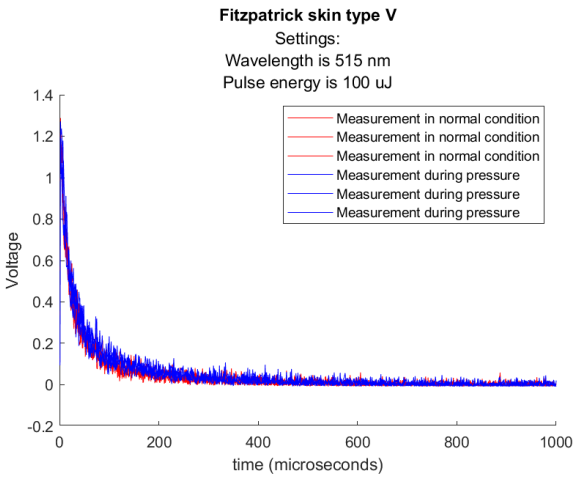

(f) Test subject with Fitzpatrick scale V
Excitation wavelength: 515 nm; pulse energy: 100 μJ

Figure 10: Validation of the excitation wavelengths 415 nm and 515 nm in three test subjects

3.2 Detector

During the first experiments for this subproject, we investigate the characteristics of detector A. One band-pass filter of 635/20 nm is mounted to the detector. The laser fiber is positioned behind the detector and both are covered using a cardboard box. Figure 11 illustrates the enormous saturation of detector A caused a by short laser pulse of approximately 20 ns. The detector directly reaches the maximum voltage of 5 V - corresponding with 5 boxes of 1 V on the vertical axis in Figure 11 - and then is blinded. Recovery takes ±8 µs (±1.5 box of 5 µs on the horizontal axis), after which it decays. However, it appears that both duration of the oversaturation and the lifetime after recovery increase with the amount of light.

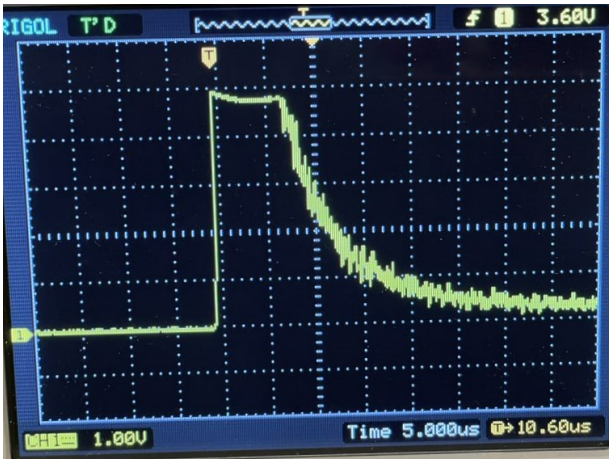

Figure 11: Visualization of oversaturated detector A One box represents 5 µs on the horizontal axis, and 1 V on the vertical axis.

Clearly, detector A experiences too much light to properly function. We experiment with various band-pass, long-pass, and absorptive filter combinations to reduce the incoming light. Figure 44 in the Appendix displays 22 measurements using one or more filters. Some of the combinations of filters produced unusual decay curves, extremely low signals, or signals primarily made up of noise. Combinations showing the most promising decay curves were executed using the filters combinations: 1x 635/20 nm, 3x 660/40 nm, 1x 635 nm + 1x >610 nm, 3x 660/40 nm + 1x >610 nm, 1x 635 nm + 1x >610 nm + 1x colored glass filter >590 nm and 1x neutral density filter.

The oversaturation is also seen in measurements in human skin, shown in Figure 12. Two detectors, covered with 635/20 nm and 660/40 nm filters are placed on skin without ALA. Little to no signal was expected, but a peak at 5 V, recovery period of ±10 µs and a decay curve are seen. Different (combinations of) band-pass, long-pass, and absorptive filters, as well as different positions of the laser fiber, are tested, but no setup could prevent the oversaturation. Measurements on skin with ALA, with an inflated and deflated blood pressure band, did not deviate from Figure 12. The measured lifetime is therefore not oxygen-dependent, indicating that the measured lifetime is not reliable and does not correspond with the oxygen tension in the mitochondria.

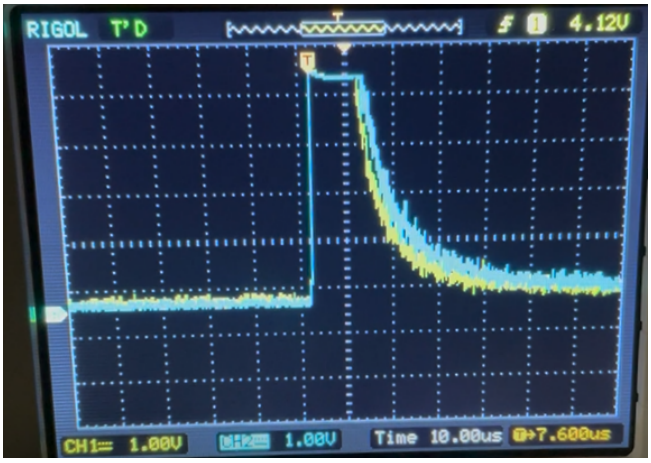

Figure 12: Oversaturated detectors in skin without ALA Yellow: detector A with 635/20 nm filter, blue: detector A with 660/40 nm filter. One box represents 10 µs on the horizontal axis, and 1 V on the vertical axis.

3.3 Light source

The first experiment in this subproject is performed in a 10 µM PpIX solution. Light source B is used. The photomultipliers are gated with a delay of 5 µs. There were no visual differences in the measured lifetimes between the test tube containing PpIX dissolved in DMF and the test tube containing DMF alone despite varying positions of the light source and the detector. It is probably because the light source and detector were not close enough to each other. We did not add a reductant such as sodium dithionite because it could not be combined with the non-aqueous solution of DMF. Therefore we could not easily minimize the PO_2 to study the oxygen-dependency of the signal.

Subsequently, experiments in human skin are performed with light sources A and B coupled into a fiber. This way, the light source and detector excite and detect the same area of the skin. First, measurements are performed with light source B, whose settings are described in the Confidential Appendix. Figure 13 shows measurements on the skin without ALA (a), on the skin with ALA and inflated blood pressure band (b), and on the skin with ALA and deflated blood pressure band (c). The signal on the skin without ALA is minimal, as expected. During the deoxygenated condition, the lifetime is increased compared to the oxygenated condition, indicating oxygen-dependency. Nevertheless, the signal increases first, which is unusual. Therefore, we should further optimize settings such as the gating period and the gain of the photomultiplier.

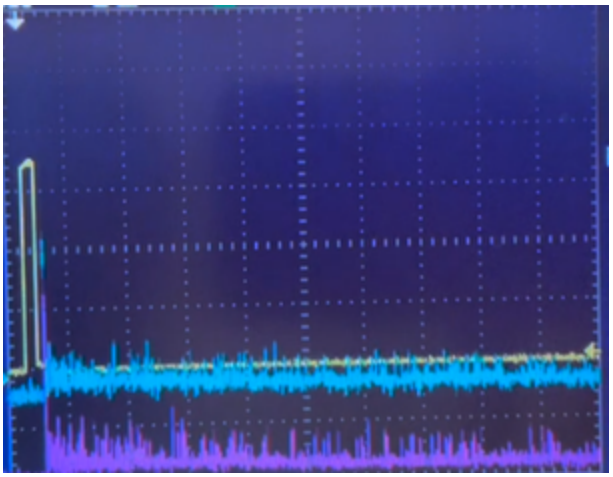

(a) Skin without ALA

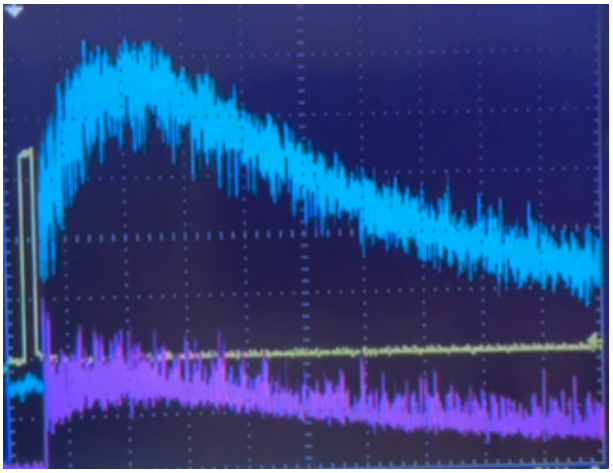

(b) Skin with ALA, microcirculation closed

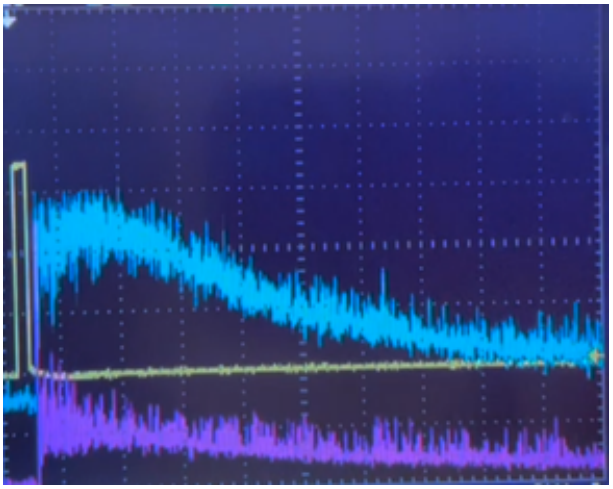

(c) Skin with ALA,microcirculation restored

Figure 13: Human skin measurement with light source B
One box on the horizontal axis represents 100 µs.
Yellow: light source B, one vertical box represents 5 mV.
Blue: photomultiplier with a detection wavelength of 635 nm, one vertical box represents 50 mV.
Magenta: photomultiplier with a detection wavelength of 660 nm, one vertical box represents 50 mV.

In order to optimize these settings, several measurements are performed with light source A and light source B. An example of these measurements can be found in Figure 14. The corresponding settings are listed in the Confidential Appendix. First, signals are recorded during the normal, oxygenated state. Then, the blood pressure band is inflated for at least 30 seconds. Signals are recorded during this deoxygenated state. The blood pressure band is deflated and measurements are performed after approximately 4 and 8 seconds. In Figure 14a the raw data and corresponding rectangular fits are shown. Since these are individual measurements, they are not averaged and contain some noise. The rectangular fits are shown in Figure 14b. The lifetime during absence of oxygen is enlarged compared with the oxygenated condition. During the deflation of the blood pressure band, the oxygen influx is restored and the lifetime is shortened.

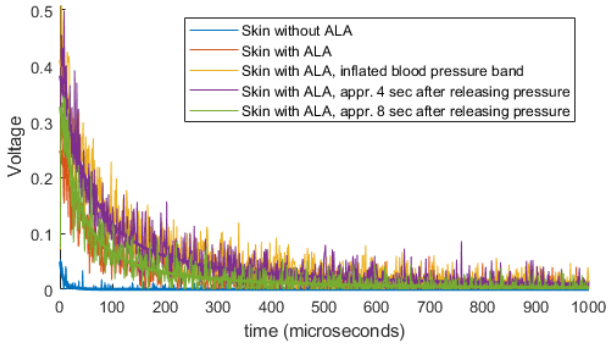

(a) Measured data and rectangular fit

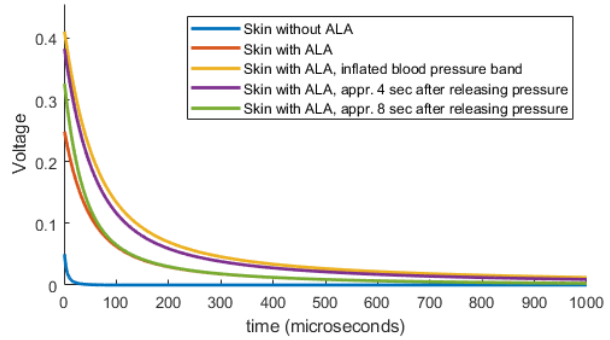

(b) Rectangular fit only

Figure 14: Measurement of human with light source A

Additional measurements were performed with light sources A and B with different settings. Six measurements with light sources A and B are shown in Figure 22 in the Confidential Appendix. All measurements were performed on the same test subject (Fitzpatrick skin type II) on the same day. A large difference is seen between measurements on the skin with and without ALA. An oxygen-dependency can be seen between measurements with closed and restored microcirculation. Additional results can be found in the Confidential Appendix.

4. DISCUSSION

In this project, we explored possibilities for improvement of the clinical device to non-invasively measure mitochondrial oxygen tension. The project is divided into three smaller projects, focusing on the excitation wavelength, detector, and light source. We will discuss the key findings, similarities, and contrasts with existing knowledge and ideas for future research per subproject.

4.1 Excitation wavelength

In the first subproject regarding the excitation wavelength, we performed three experiments. In the first experiment, we explored wavelengths in the spectrum of 415 to 695 nm. We found that the wavelengths 415, 515, 530, and 635 nm could potentially be used as excitation wavelengths, because these measurements contained little noise and the rectangular fits represented the data points accurately. These wavelengths were further examined in a second experiment using a situation with and a situation without oxygen. We saw oxygen-dependent lifetimes containing only a small amount of noise for the excitation wavelengths 415 and 515 nm. Then, in the third experiment, we tested these two wavelengths on three test subjects with various skin types. For the test subjects with Fitzpatrick skin types II and IV, an oxygen-dependent lifetime was found for both 415 nm and 515 nm. In the darker skin type V, an oxygen-dependent lifetime was only found using a wavelength of 415 nm.

This suggests the potential use of 415 nm as excitation wavelength for all tested skin types. As shown in Figure 4, the absorption spectrum of PpIX shows a large peak around 405 nm compared to a 10 times smaller peak around 515 nm.[27] This difference in absorbed energy between 415 nm and 515 nm is also found in our experiments, because the required pulse energy for 415 nm is 10-20 µJ, while 100 µJ is required for 515 nm measurements.

However, differences can be seen between the measurements of the test subjects. The 515 nm measurement with 100 µJ shows clipping during the first 50 µs in the test subject with skin type II, indicating the photomultipliers are saturated. The successive lifetime is long, potentially due to the recovery of the oversaturated photomultipliers. This might be avoided by reducing the gain or lowering the pulse energy. This clipping leads to an incorrect rectangular fit, which will result in an inaccurate mitoPO$_2$ calculation. In the test subject with skin type V, considerably shorter lifetimes were found. In this test subject, the 515 nm measurement does not reveal any oxygen-dependency. Possibly, not enough pressure is applied to the probe, which leaves the microcirculation partially open. Moreover, a comparison to measurements in the skin without ALA is recommended in future research. We expect minimal to no signal in the skin without ALA, and this could serve as validation for the lifetimes measured in the skin that contains ALA. If the signal in the skin without ALA is comparable to the measurements in the skin with ALA, the measured signal cannot be delayed fluorescence, but rather artifacts, noise, or electrical lifetimes of the used components, resulting in inaccurate mitoPO$_2$ calculations.

The various test subjects required different pulse energies in the 415 nm measurements to avoid noise but prevent oversaturation. A pulse energy of 10 µJ did not cause oversaturation for test subjects with Fitzpatrick's skin type II and IV, while 20 µJ was required for test subject with skin type V to prevent noise. This could be explained by the Opolette's instability. Although the Opolette's Q-Switch delay was set as low as was possible in an effort to stabilize it, there was still a 20% difference in the observed pulse energy between individual samples.

Since we only measured three test subjects with different skin types, we cannot state that the differences between the measured lifetimes are caused by the different skin types. MitoPO$_2$ measurements differ a lot between humans.[19,33] Therefore, a larger validation study with more test subjects, representing all six Fitzpatrick skin types, is required to test whether the differences between lifetimes measured with 415 nm and 515 nm can be assigned to the skin types.

A wavelength of 415 nm is used as minimum wavelength. According to the PpIX absorption spectrum in Figure 4, even more photons are absorbed using 405 nm. The minimum wavelength of the Opolette 355 tunable laser is 410 nm, so we were not able to measure using a wavelength of 405 nm. Moreover, pulse energies at 410 nm were very unstable. Therefore, 415 nm is chosen as minimum wavelength.

So, it is technically possible to obtain oxygen-dependent lifetimes with an excitation wavelength of 415 nm. However, the clinical relevance of 415 nm as the excitation wavelength should be further investigated. The skin consists of three layers, with the epidermis being the most superficial layer, followed by the dermis and hypodermis.[34] The average thickness of the epidermis is 74.9 (±12.7) µm, and the epidermis and dermis together are 2.12 mm thick.[35,36] Light with a wavelength of 515 nm penetrates deeper into the skin than 415 nm, but the exact penetration depths vary in the available literature. Avci *et al.* indicated that violet to deep blue light (wavelength 390-470 nm) penetrates the skin ±0.3 mm and blue to green light (wavelength 475-545 nm) ±0.3-0.5 mm.[28] This differs

from Clement *et al.*, showing penetration depths of ±1 mm and ±2.5 mm for blue (wavelength 440 nm) and green light (wavelength 540 nm), respectively. These wavelengths differ slightly between the studies so an exact comparison is not possible, but the reported penetration depths are inconsistent. The exact penetration depth is relevant because the penetration depth of 415 nm could be close to the thickness of the epidermis. This could mean that the 415 nm measurements are performed in the epidermis, which has a different structure and function than the dermis. The COMET excites light with a wavelength of 515 nm to measure the delayed fluorescence of PpIX in the dermis, and measurements in the epidermis could result in insufficient mitoPO_2 values. In addition, 415 nm measurements are more superficial and potentially more susceptible to differences in environmental oxygen or ambient light. Therefore, further research is indicated to validate the results using 415 nm as excitation wavelength in the clinic.

4.2 Detector

In the second subproject, we investigated the possibilities of using detector A. Detector A was tested under various conditions. We found an oversaturation of the detector. An attempt was made to prevent this saturation using (combinations of) band-pass, long-pass, and absorptive filters. This resulted in six potential combinations of filters. Human skin measurements also oversaturated in all setups with different filters and positions.

Several filter combinations were investigated using the fluorescent PdP with unknown concentration and volume. This was not ideal due to the chosen setup and the differences between PdP and PpIX. Detector A was positioned about 3 centimeters away from the laser. The PdP solution probably absorbs all the laser light superficially, which means that detector A probably never receives the delayed fluorescence signal. In addition, the emission spectra of PdP and PpIX differ. A PpIX solution or human skin should be used to repeat this experiment to investigate combinations of filters.

Detector A has the potential to be used in the COMET, as it is very sensitive and small. However, oversaturation is a major problem for detector A. Oxygen-dependent lifetimes could not be obtained in the measurements on human skin due to the recovery period of the detector. A configuration, as described in the Confidential Appendix, is constructed to prevent this, but is not yet completed.

4.3 Light source

In subproject three, we experimented with a new kind of light source. In test tubes, no differences in results were found between a solution of PpIX in solvent and solvent only, probably because of our bulky prototypes and the impossibility to find an ideal position. For measurements in human skin, we coupled the light sources into a fiber. These measurements showed oxygen-dependent lifetimes and a large difference in intensity between skin prepared with ALA and unprepared skin. These results indicate that we actually detect delayed fluorescence with light source A and light source B.

The ALA application time affects the maximum amplitude. In previous studies, an ALA application time of at least 3 hours was recommended.[5,10] For both light sources A and B, we see higher amplitudes with longer ALA application time. According to the Dutch Medicines Evaluation Board, the fluorescence signal is highest 6 hours after application of the ALA adhesive and reaches its baseline level after 48 hours.[37]

4.4 Future

In this work, possible improvements regarding the COMET are investigated separately. When all components are further optimized, these components can be combined into one prototype. The use of the investigated components provides opportunities to change the design of the COMET device. Currently, the device is attached to a mobile cart, and a rigid cable with a sensitive fiber connects the skin probe to the device. In my experience, this is impractical in the operating room. The device is positioned as far from the patient as possible, to leave space for everyone to work near the patient. This frequently results in a tightly strung cable, which is not conducive to the measurements. Light sources A and B and detector A are much smaller and lighter than the Q-Switched laser and photomultiplier of the COMET. A device with these small components may be able to be placed directly on the measurement site, eliminating the fiber from the device to the skin. However, attention should be taken to avoid the application of unwanted pressure on the skin. Placing a device on the skin may partially occlude the microcirculation, resulting in inaccurate measurements. Another idea is to attach a small device on the skin near the measurement site and connect it to a probe via a small fiber. Other drawbacks of the Q-Switched laser were the frequently occurring laser failures. Light sources A and B are based on a relatively simple technique, as explained in the Confidential Appendix. Therefore, they could be more reliable, but this requires further validation.

Further research is recommended to improve the components of the existing COMET device. As a first step, we suggest to focus on the excitation wavelength of 415 nm. To validate the 415 nm measurements, multiple test subjects with skin types varying from type I to VI on the Fitzpatrick scale should be measured with

both 415 nm and 515 nm. Detector A currently cannot replace the photomultiplier. However, we worked on a configuration as described in the Confidential Appendix, but due to time constraints we were not able to perform tests. This configuration should be completed and the possibilities for use should be explored. For light sources A and B, varying parameters are investigated, but more research is necessary before drawing firm conclusions about these parameters. Ultimately, a prototype might be constructed by combining the three subprojects. The reliability and practicality of this prototype should be researched and compared to the existing COMET device.

5. CONCLUSION

This work investigates possible improvements to a clinical device for non-invasive measurement of mitochondrial oxygen tension. The device is based on the PpIX-TSLT. A light pulse excites PpIX in mitochondria, resulting in a delayed fluorescence signal whose lifetime depends on the amount of oxygen present. In this work, improvements in excitation wavelength, detector, and light source are investigated. At an excitation wavelength of 415 nm, oxygen-dependent delayed fluorescence signals are observed in all skin types tested. A new detector is investigated to replace the large and expensive photomultipliers, but it was oversaturated due to the light pulse generated by the laser pulse. The novel light sources showed oxygen-dependent lifetimes, indicating their potential to be used for this application. These components need further research before they can be combined into a working prototype.

REFERENCES

1. Carreau A, Hafny-Rahbi BE, Matejuk A, Grillon C, Kieda C. Why is the partial oxygen pressure of human tissues a crucial parameter? Small molecules and hypoxia. *Journal of Cellular and Molecular Medicine.* 2011;15:1239-1253.
2. Reich D, Wahr JA, Tremper KK, Samra S, Delpy DT. Emerging Technologies Near-Infrared Spectroscopy: Theory and Applications. *Journal of Cardiothoracic and Vascular Anesthesia.* 1996;10:406-418.
3. Pittman R. *Regulation of Tissue Oxygenation.* Morgan & Claypool Life Sciences 2011.
4. Cooper G. The mechanism of oxidative phosphorylation. *The Cell: A Molecular Approach.* 2000:396–402.
5. Mik EG, Stap J, Sinaasappel M, *et al.* Mitochondrial PO2 measured by delayed fluorescence of endogenous protoporphyrin IX. *Nature Methods.* 2006;3:939-945.
6. Brand MD, Nicholls DG. Assessing mitochondrial dysfunction in cells. *Biochemical Journal.* 2011;435:297-312.
7. Simonson SG, Piantadosi CA. Monitoring Cardiac Function and Tissue Perfusion Near-Infrared Spectroscopy - Clinical Applications. *Critical Care Clinics.* 1996;12.
8. Borden WT, Hoffmann R, Stuyver T, Chen B. Dioxygen: What Makes This Triplet Diradical Kinetically Persistent? *Journal of the American Chemical Society.* 2017;139:9010-9018.
9. Mik EG. Measuring mitochondrial oxygen tension: From basic principles to application in humans. *Anesthesia and Analgesia.* 2013;117:834-846.
10. Harms FA, Boon WM, Balestra GM, *et al.* Oxygen-dependent delayed fluorescence measured in skin after topical application of 5-aminolevulinic acid. *Journal of Biophotonics.* 2011;4:731-739.
11. Früngel FB. *Optical Pulses-Lasers-Measuring Techniques.* Academic Press 2014.
12. Ubbink R, Wefers Bettink MA, Janse R, *et al.* A monitor for Cellular Oxygen METabolism (COMET): monitoring tissue oxygenation at the mitochondrial level. *Journal of Clinical Monitoring and Computing.* 2017;31:1143-1150.
13. Mik EG, Johannes T, Zuurbier CJ, *et al.* In vivo mitochondrial oxygen tension measured by a delayed fluorescence lifetime technique. *Biophysical Journal.* 2008;95:3977-3990.
14. Mik EG, Ince C, Eerbeek O, *et al.* Mitochondrial oxygen tension within the heart. *Journal of Molecular and Cellular Cardiology.* 2009;46:943-951.
15. Wefers Bettink MA, Harms FA, Dollee N, *et al.* Non-invasive versus ex vivo measurement of mitochondrial function in an endotoxemia model in rat: Toward monitoring of mitochondrial therapy. *Mitochondrion.* 2020;50:149-157.
16. Mandigers L, Pooth JS, Wefers Bettink MA, *et al.* Monitoring Mitochondrial Partial Oxygen Pressure During Cardiac Arrest and Extracorporeal Cardiopulmonary Resuscitation. An Experimental Pilot Study in a Pig Model. *Frontiers in Cardiovascular Medicine.* 2021;8.
17. Mik EG, Balestra GM, Harms FA. Monitoring mitochondrial PO2: the next step. *Current opinion in critical care.* 2020;26:289-295.
18. Römers LH, Bakker C, Dollée N, *et al.* Cutaneous mitochondrial PO2, but not tissue oxygen saturation, is an early indicator of the physiologic limit of hemodilution in the pig. *Anesthesiology.* 2016;125:124-132.
19. Harms F, Stolker RJ, Mik E. Cutaneous respirometry as novel technique to monitor mitochondrial function: A feasibility study in healthy volunteers. *PLoS ONE.* 2016;11.
20. Dijk LJ, Ubbink R, Terlouw LG, Noord D, Mik EG, Bruno MJ. Oxygen-dependent delayed fluorescence of protoporphyrin IX measured in the stomach and duodenum during upper gastrointestinal endoscopy. *Journal of Biophotonics.* 2019;12.
21. Harms FA, Brandt-Kerkhof AR, Mik EG. Monitoring of mitochondrial oxygenation during perioperative blood loss. *BMJ Case Reports.* 2021;14.
22. Baumbach P, Schmidt-Winter C, Hoefer J, *et al.* A Pilot Study on the Association of Mitochondrial Oxygen Metabolism and Gas Exchange During Cardiopulmonary Exercise Testing: Is There a Mitochondrial Threshold? *Frontiers in Medicine.* 2020;7.
23. Costerus SA, Wefers Bettink M, Tibboel D, Graaff JC, Mik EG. Mitochondrial Oxygen Monitoring During Surgical Repair of Congenital Diaphragmatic Hernia or Esophageal Atresia: A Feasibility Study. *Frontiers in Pediatrics.* 2020;8.
24. Neu C, Baumbach P, Plooij AK, *et al.* Non-invasive Assessment of Mitochondrial Oxygen Metabolism in the Critically Ill Patient Using the Protoporphyrin IX-Triplet State Lifetime Technique—A Feasibility Study. *Frontiers in Immunology.* 2020;11.
25. Conversion factors and tables [Online]. Available from: https://dokumen.tips/documents/bs350-conversion-factors-and-tables.html?page=1. Assessed: 2022-11-18.
26. Harms FA, Bodmer SI, Raat NJ, Mik EG. Cutaneous mitochondrial respirometry: non-invasive monitoring of mitochondrial function. *Journal of Clinical Monitoring and Computing.* 2015;29:509-519.
27. Falk J. *Porphyrins and Metalloporphyrins; Their General, Physical and Coordination Chemistry, and Laboratory Methods.* B.B.A. Library, V.2Elsevier Publishing Company 1964.
28. Avci P, Gupta A, Sadasivam M, *et al.* Low-level laser (light) therapy (LLLT) in skin: stimulating, healing, restoring. *Seminars in cutaneous medicine and surgery.* 2013;32 1:41-52.
29. Clement M, Daniel G, Trelles M. Optimising the design of a broad-band light source for the treatment of skin *Journal of Cosmetic and Laser Therapy.* 2005;7(3-4):177-189.
30. Mantri Y, Jokerst JV. Impact of skin tone on photoacoustic oximetry and tools to minimize bias *Biomedical Optics Express.* 2022;13:875.
31. Fitzpatrick T. Soleil et peau [Sun and Skin] *J. Med Esthetique.* 1975;2:33-4.
32. Hamamatsu . Photomultiplier tube module H11526-20. [Online]. Available from: https://www.hamamatsu.com/eu/en/product/optical-sensors/pmt/pmt-module/current-output-type/H11526-20.html. Assessed: 2022-10-19.

33. Ubbink R, Wefers Bettink MA, Weteringen W, , Mik EG. Mitochondrial oxygen monitoring with COMET: verification of calibration in man and comparison with vascular occlusion tests in healthy volunteers. *Journal of Clinical Monitoring and Computing.* 2021;35:1357-1366.

34. Yousef H, Alhajj M, Sharma S. *Anatomy, Skin (Integument), Epidermis.* StatPearls 2022.

35. Sandby-Møller J, Poulsen T, Wulf H. Epidermal thickness at different body sites: relationship to age, gender, pigmentation, blood content, skin type and smoking habits *Acta Derm Venereol.* 2003;83(6):410-413.

36. Van Mulder T, de Koeijer M, Theeten H, *et al.* High frequency ultrasound to assess skin thickness in healthy adults *Vaccine.* 2017;35(14):1810-1815.

37. Alacare 8 mg cutaneous adhesive. [Online]. Available from: https://www.geneesmiddeleninformatiebank.nl/nl/rvg113539. Assessed: 2022-11-19.

LIST OF ABBREVIATIONS

ALA	5-aminovulinic acid hydrochloride
ATP	Adenosine triphosphate
COMET	Cellular oxygen metabolism
DMF	Dimethylformamide
mitoPO_2	Mitochondrial oxygen tension
mmHg	Millimeters of mercury
PdP	Palladium porphyrin
PpIX	Protoporphyrin IX
PpIX-TSLT	Protoporphyrin IX-triplet state lifetime technique

CONFIDENTIAL APPENDIX

The Confidential Appendix is accessible only to the graduation committee, so these pages are intentionally left blank.

CONFIDENTIAL APPENDIX

The Confidential Appendix is accessible only to the graduation committee, so these pages are intentionally left blank.

CONFIDENTIAL APPENDIX

The Confidential Appendix is accessible only to the graduation committee, so these pages are intentionally left blank.

CONFIDENTIAL APPENDIX

The Confidential Appendix is accessible only to the graduation committee, so these pages are intentionally left blank.

APPENDIX

Overview of available literature about PpIX-TSLT

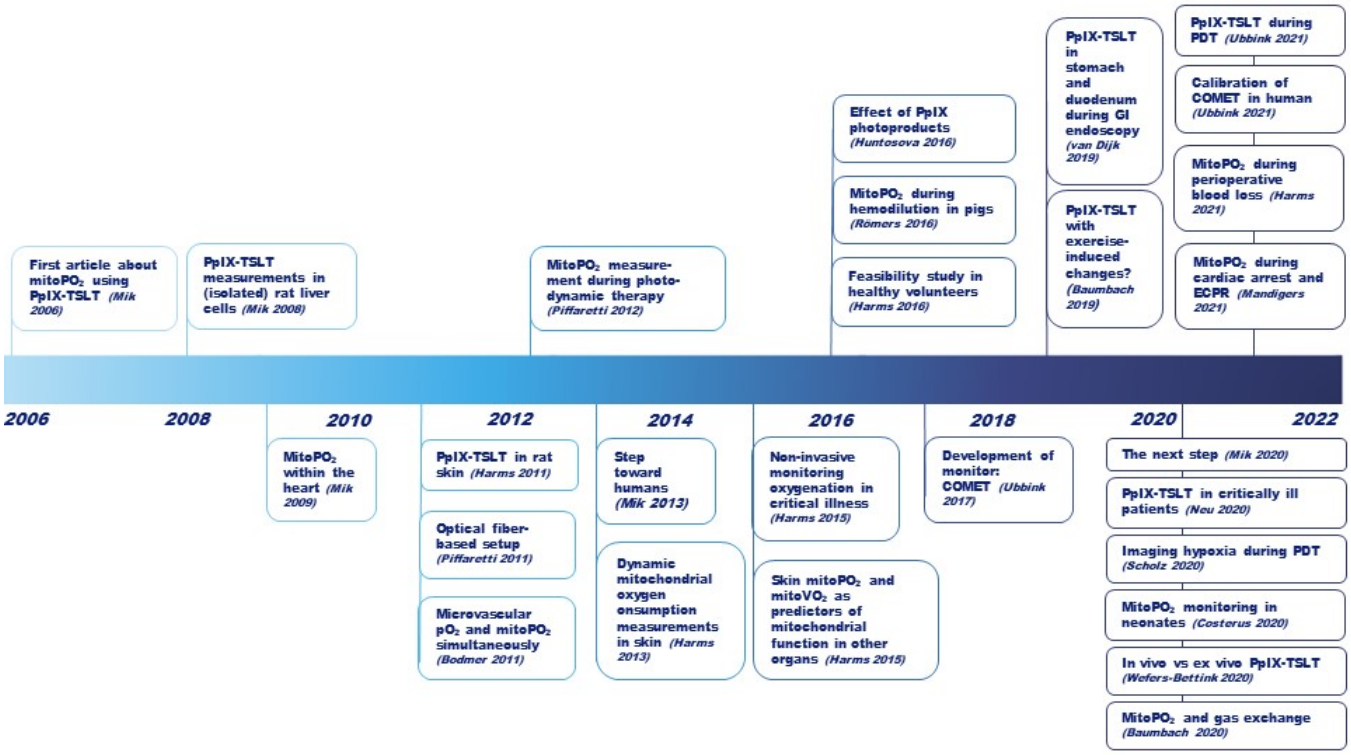

Figure 23: Overview of available literature until May 2022

Excitation wavelength

Settings to achieve equal pulse energies per excitation wavelength

Table 2: Settings to achieve equal pulse energies per excitation wavelength

Energy (µJ)	Wavelength (λ)	Filters	Percentage of original energy (%)	Q-Switch delay (µs)
10	415	0.9+0.38	5	155
	515	0.9+0.6+0.38	1.25	145
	530	0.9+0.6+0.38	1.25	158
	635	0.9+0.6+0.15	2.19	145
20	415	0.9+0.15	8.75	152
	515	0.9+0.6	3.13	165
	530	0.9+0.38+0.3	2.5	158
	635	0.6+0.38+0.3	5	150
40	415	0.6+0.15	17.5	159
	515	0.9+0.38	5	145
	530	0.9+0.38	5	160
	635	0.6+0.38	10	158
100	415	0.3+0.15	35	155
	515	0.9	12.5	150
	530	0.6+0.3	12.5	160
	635	0.6	25	160

Available filters with their transmission: 0.9 (transmission 12.5), 0.6 (25%), 0.38 (40%), 0.3 (50%), 0.15 (70%).

Rectangular fits on wavelengths between 415 and 695 nm

For the wavelengths between 415 and 695 with steps of 20 nm, three measurements are performed. The quality switch delay is set at 180 µs. The laser power is reduced to 6.25%, to avoid over saturation of the signal. This results in a different pulse energy per wavelength, and these are shown in Table 1. The measurements and corresponding rectangular fits are shown per excitation wavelength.

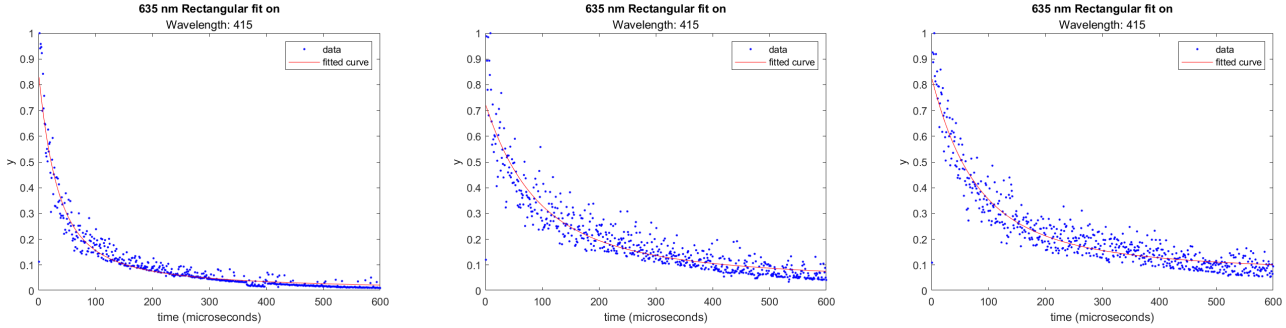

Figure 24: Three rectangular fits measured with an excitation wavelength of 415 nm.

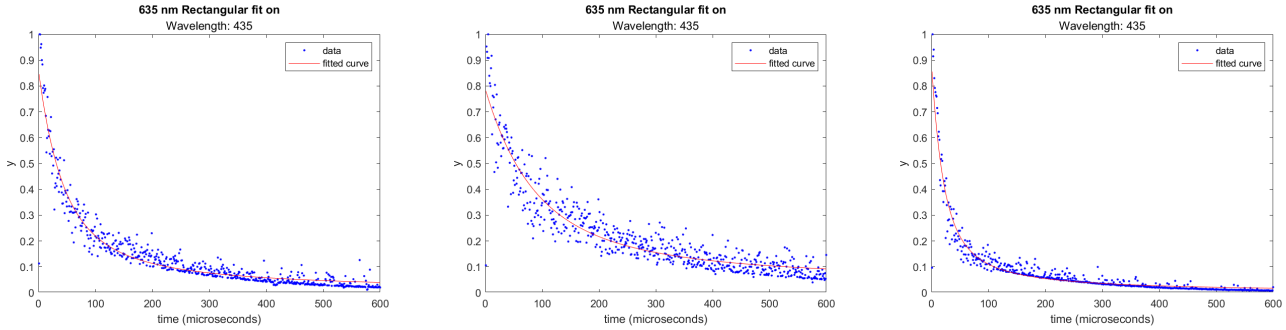

Figure 25: Three rectangular fits measured with an excitation wavelength of 435 nm.

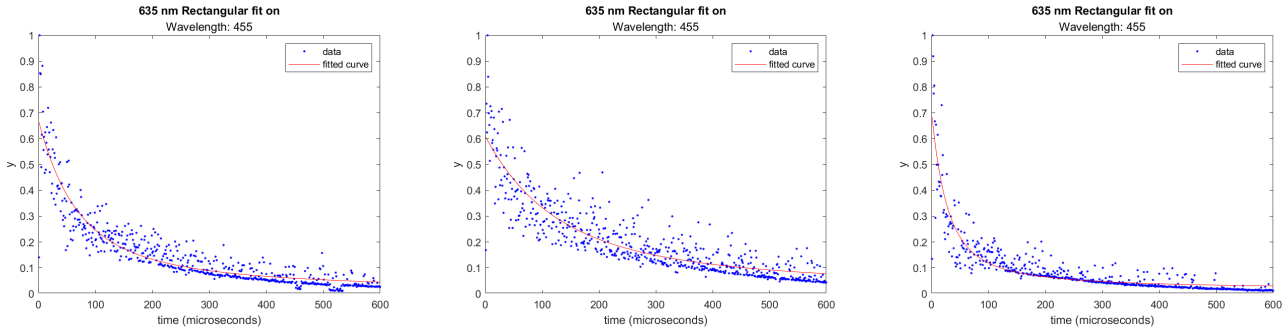

Figure 26: Three rectangular fits measured with an excitation wavelength of 455 nm.

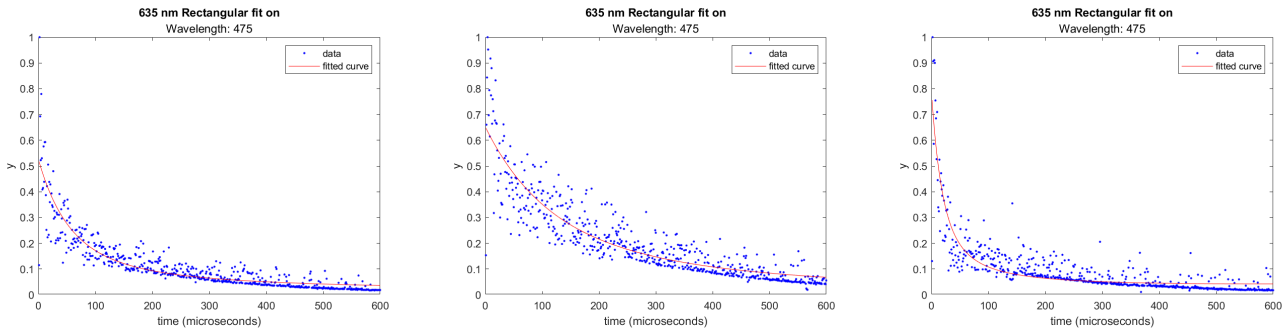

Figure 27: Three rectangular fits measured with an excitation wavelength of 475 nm.

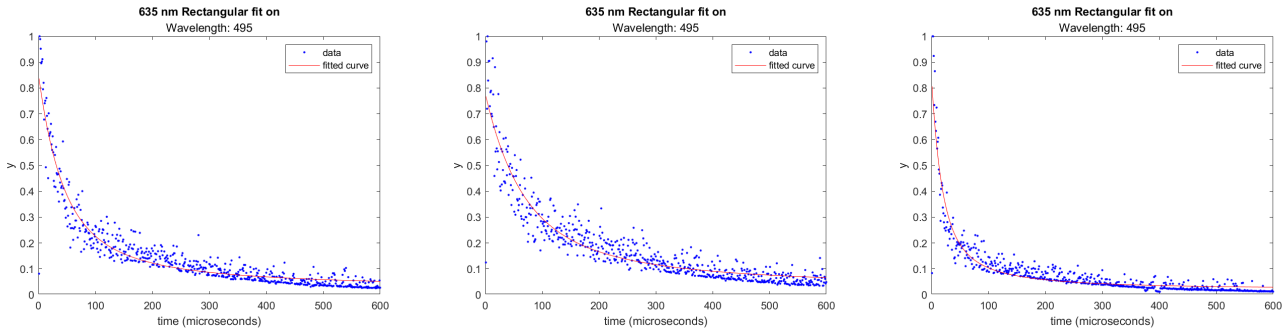

Figure 28: Three rectangular fits measured with an excitation wavelength of 495 nm.

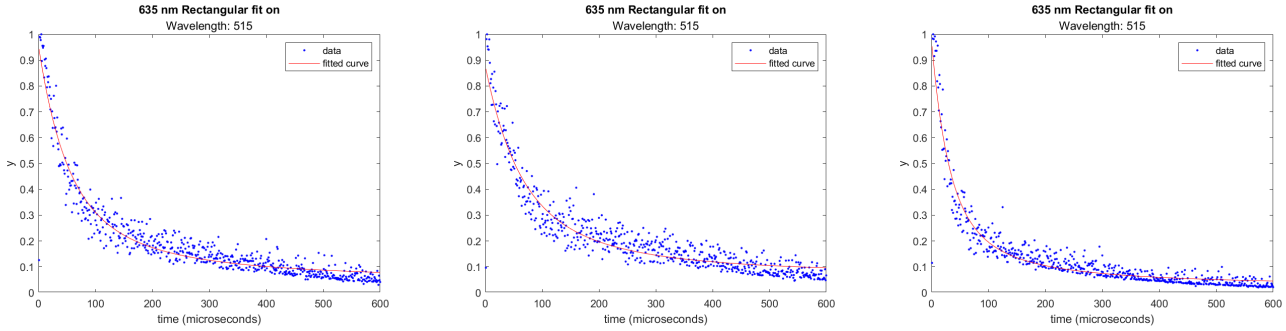

Figure 29: Three rectangular fits measured with an excitation wavelength of 515 nm.

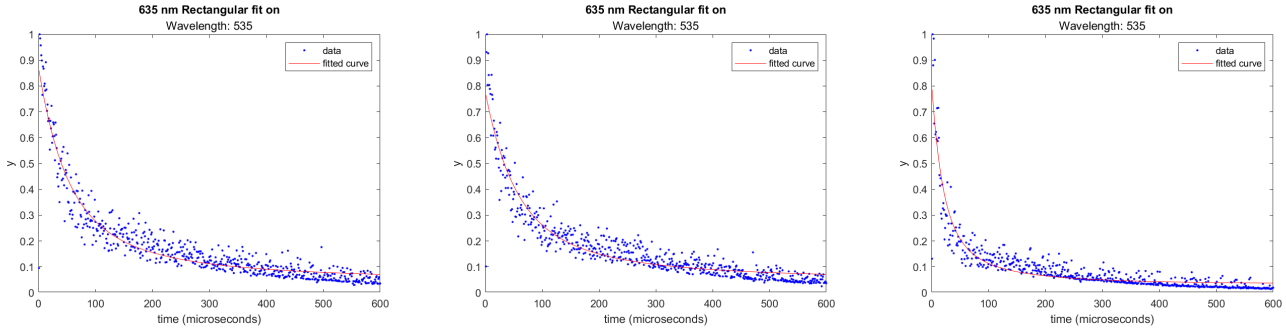

Figure 30: Three rectangular fits measured with an excitation wavelength of 535 nm.

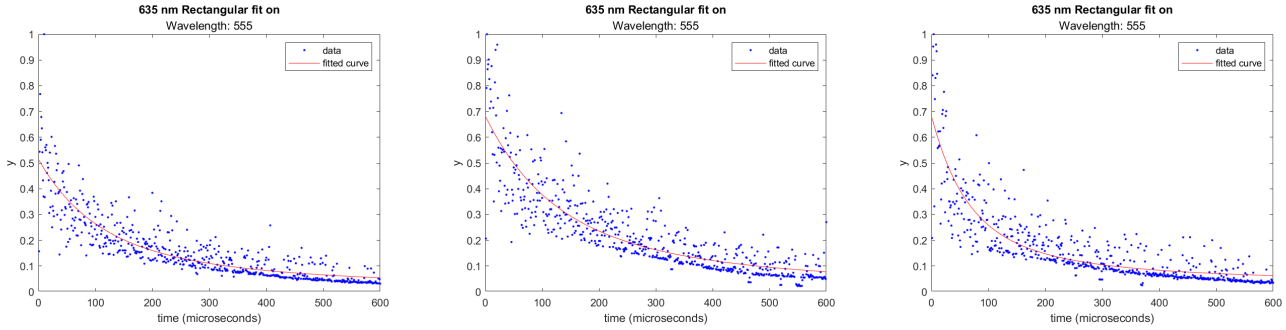

Figure 31: Three rectangular fits measured with an excitation wavelength of 555 nm.

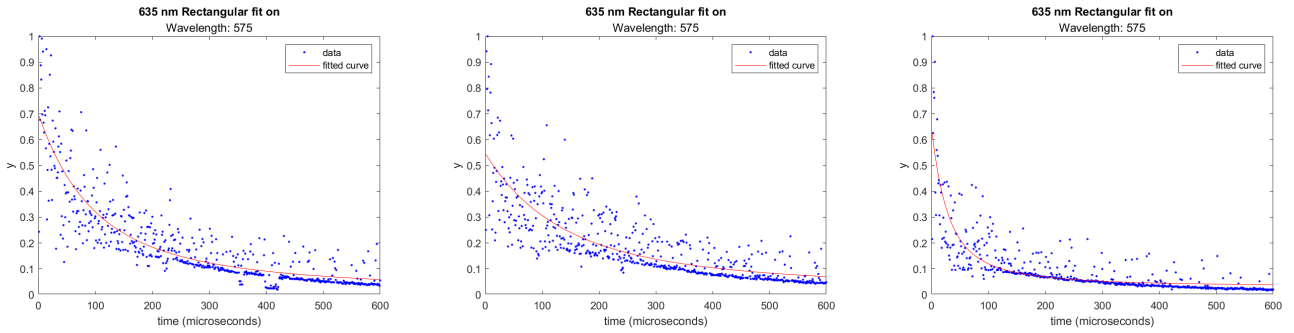

Figure 32: Three rectangular fits measured with an excitation wavelength of 575 nm.

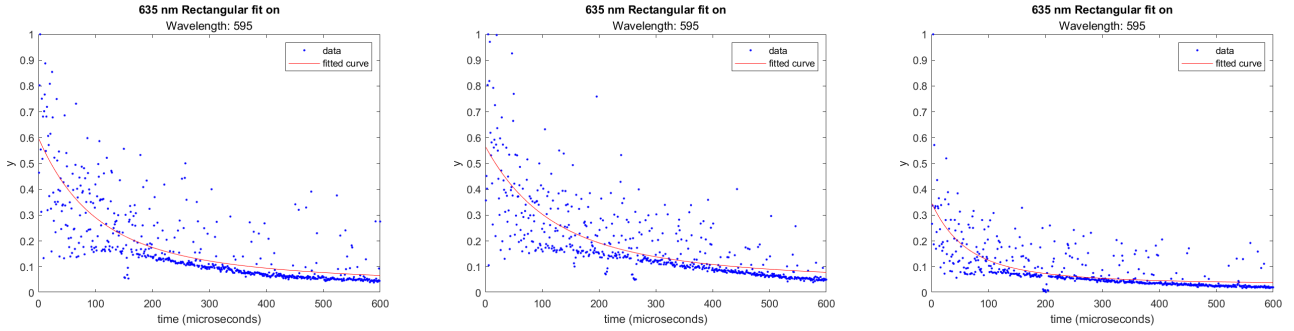

Figure 33: Three rectangular fits measured with an excitation wavelength of 595 nm.

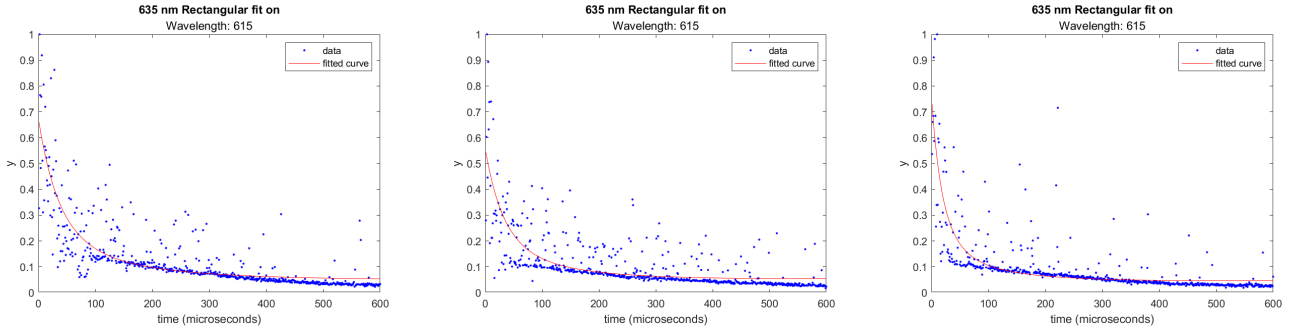

Figure 34: Three rectangular fits measured with an excitation wavelength of 615 nm.

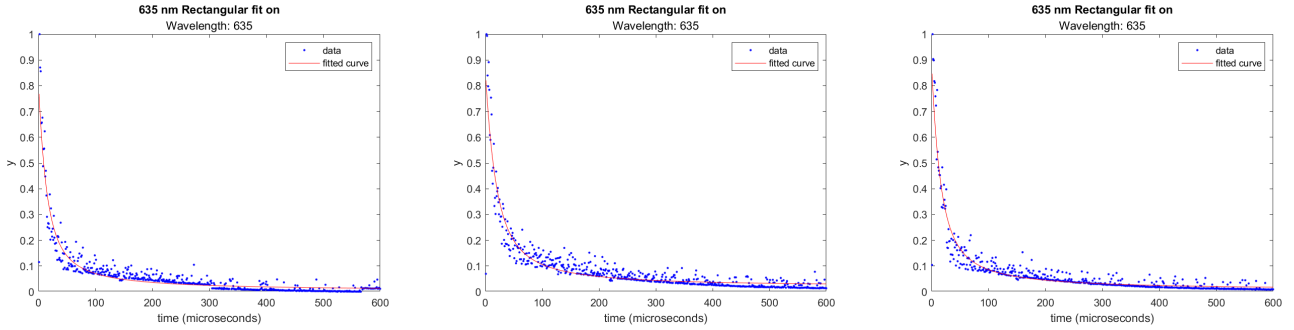

Figure 35: Three rectangular fits measured with an excitation wavelength of 635 nm.

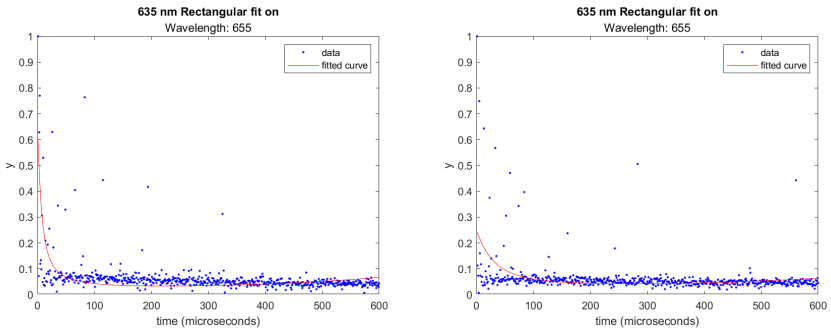

Figure 36: Two rectangular fits measured with an excitation wavelength of 655 nm.

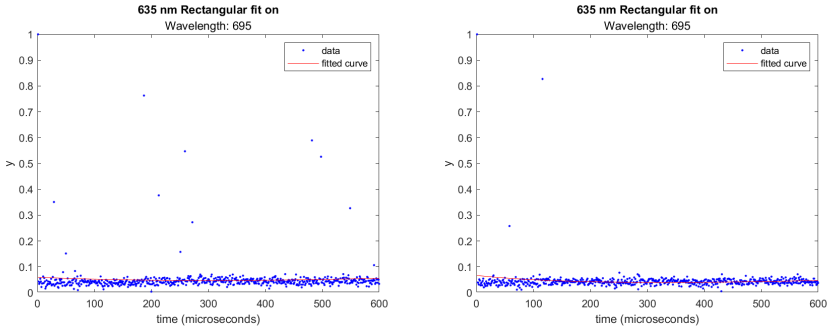

Figure 37: Two rectangular fits measured with an excitation wavelength of 695 nm.

Optimization of most promising wavelengths with varying pulse energies

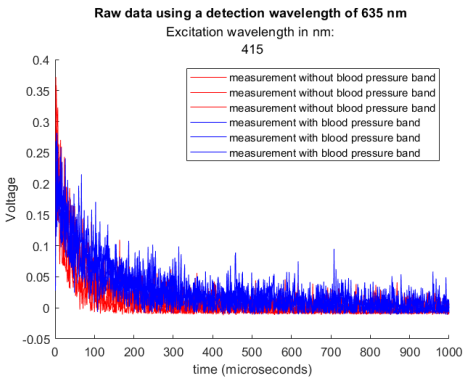

(a) Excitation wavelength: 415 nm; pulse energy: 10 µJ

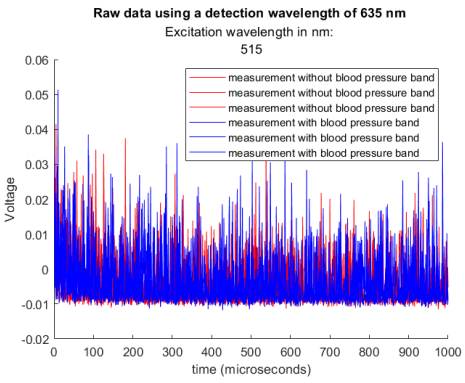

(b) Excitation wavelength: 515 nm; pulse energy: 10 µJ

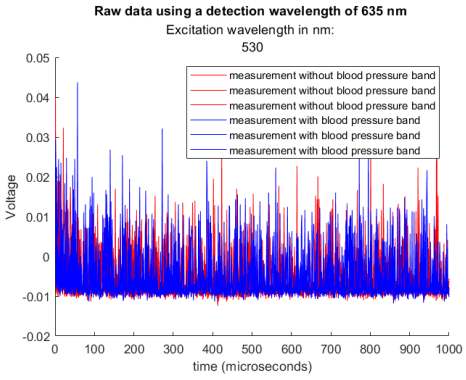

(c) Excitation wavelength: 530 nm; pulse energy: 10 µJ

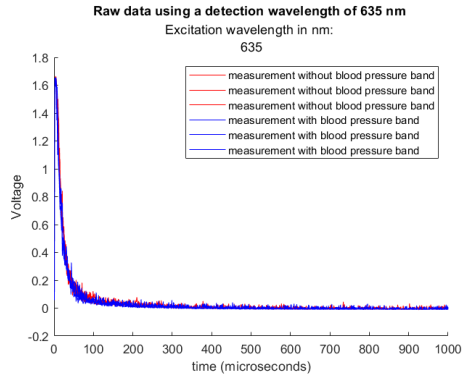

(d) Excitation wavelength: 635 nm; pulse energy: 10 µJ

Figure 38: Measurements in oxygenated and deoxygenated condition.

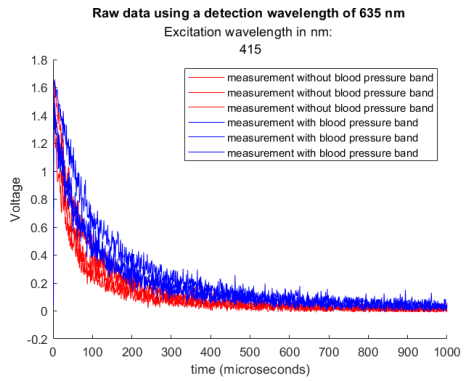

(a) Excitation wavelength: 415 nm; pulse energy: 20 µJ

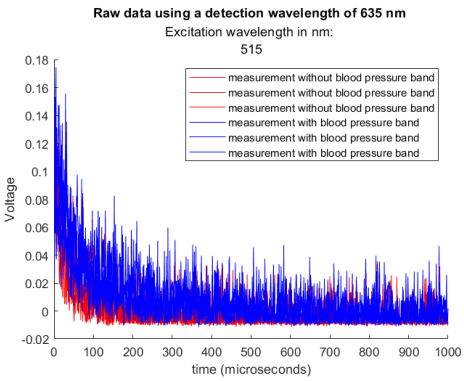

(b) Excitation wavelength: 515 nm; pulse energy: 20 µJ

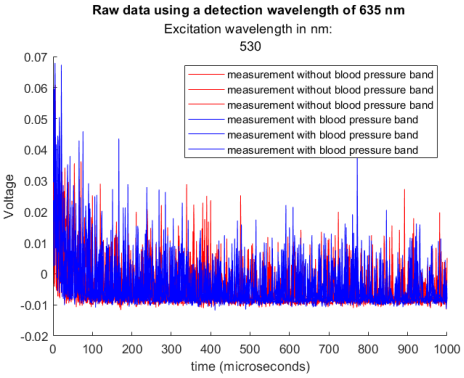

(c) Excitation wavelength: 530 nm; pulse energy: 20 µJ

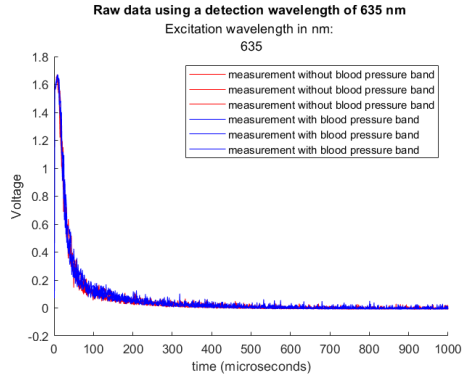

(d) Excitation wavelength: 635 nm; pulse energy: 20 µJ

Figure 39: Measurements in oxygenated and deoxygenated condition.

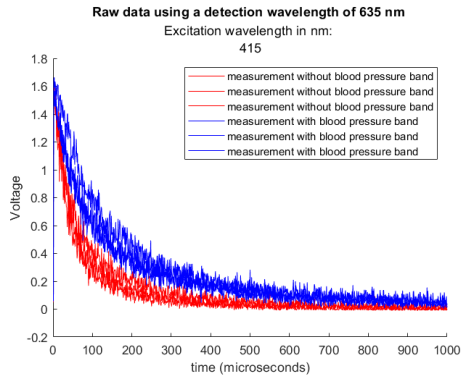

(a) Excitation wavelength: 415 nm; pulse energy: 40 µJ

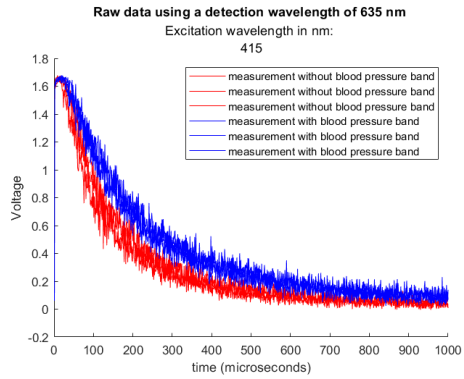

(b) Excitation wavelength: 415 nm; pulse energy: 100 µJ

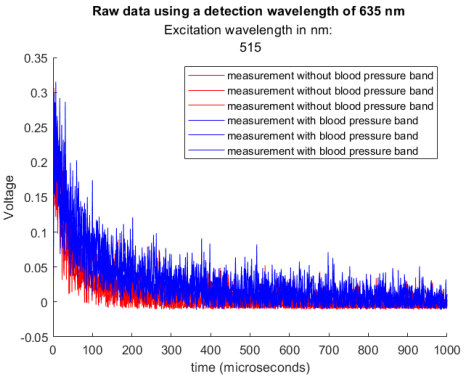

(c) Excitation wavelength: 515 nm; pulse energy: 40 µJ

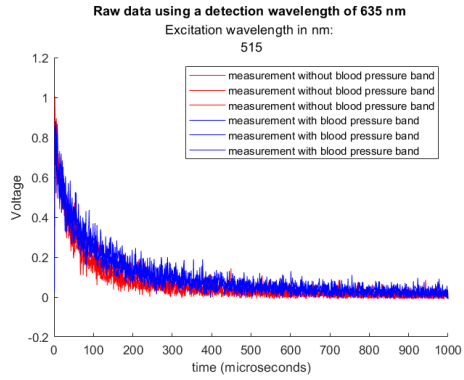

(d) Excitation wavelength: 515 nm; pulse energy: 100 µJ

Figure 40: Measurements in oxygenated and deoxygenated condition

Validation of excitation wavelengths 415 nm and 515 nm in test subjects with different skin tones

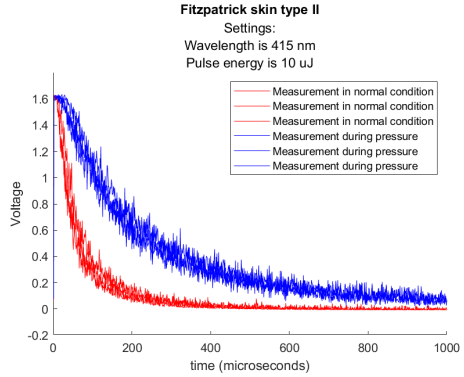

(a) Excitation wavelength: 415 nm; pulse energy: 10 µJ

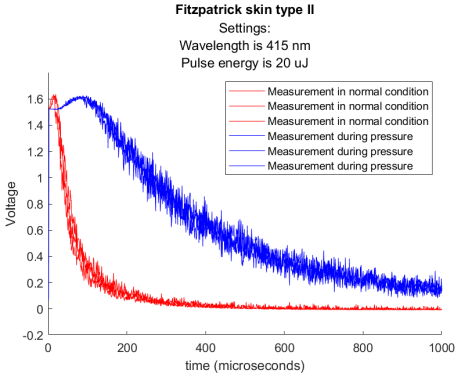

(b) Excitation wavelength: 415 nm; pulse energy: 20 µJ

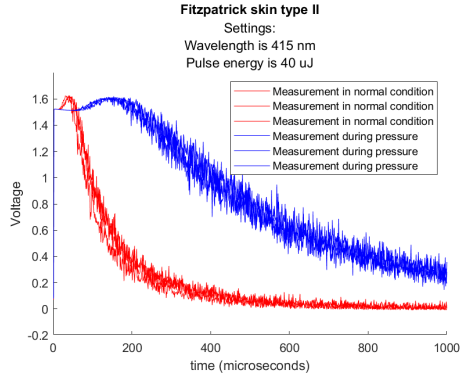

(c) Excitation wavelength: 415 nm; pulse energy: 40 µJ

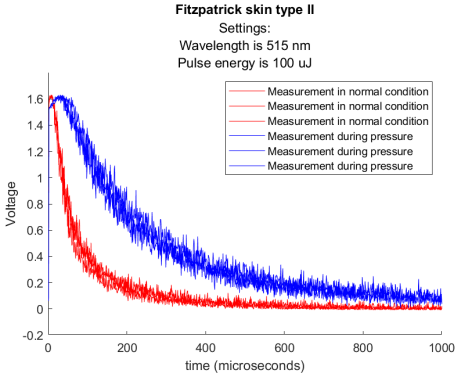

(d) Excitation wavelength: 515 nm; pulse energy: 100 µJ

Figure 41: Measurement in Fitzpatrick skin type II using 415 nm (10, 20 and 40 µJ) and 515 nm (100 µJ).

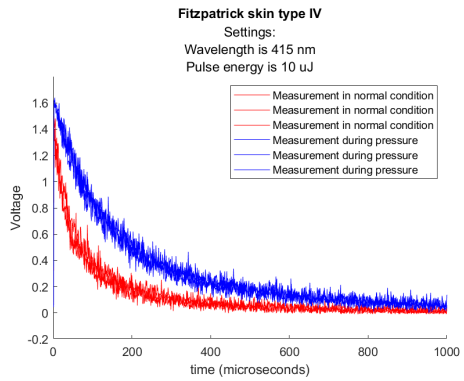

(a) Excitation wavelength: 415 nm; pulse energy: 10 µJ

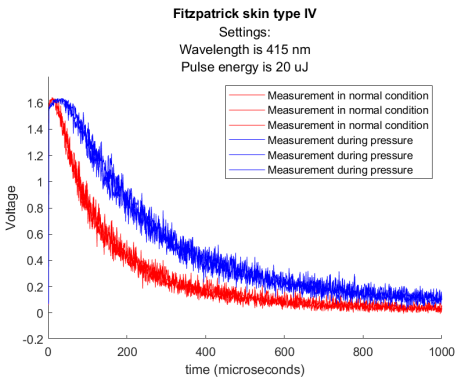

(b) Excitation wavelength: 415 nm; pulse energy: 20 µJ

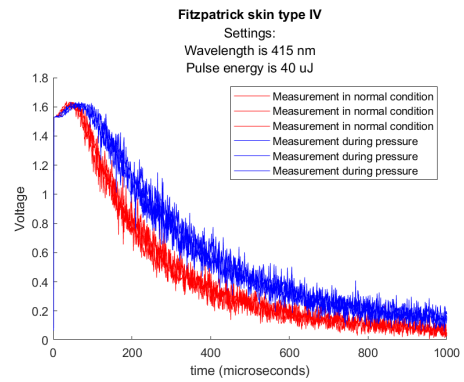

(c) Excitation wavelength: 415 nm; pulse energy: 40 µJ

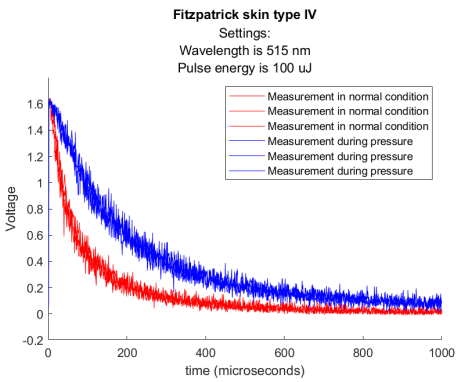

(d) Excitation wavelength: 515 nm; pulse energy: 100 µJ

Figure 42: Measurement in Fitzpatrick skin type IV using 415 nm (10, 20 and 40 µJ) and 515 nm (100 µJ).

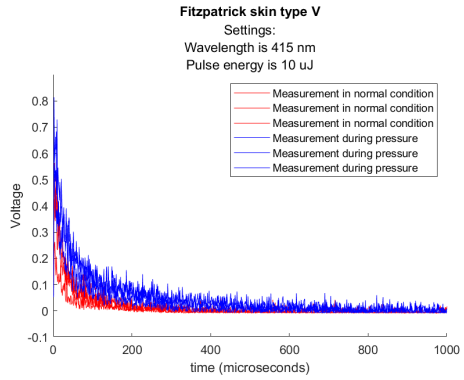

(a) Excitation wavelength: 415 nm; pulse energy: 10 μJ

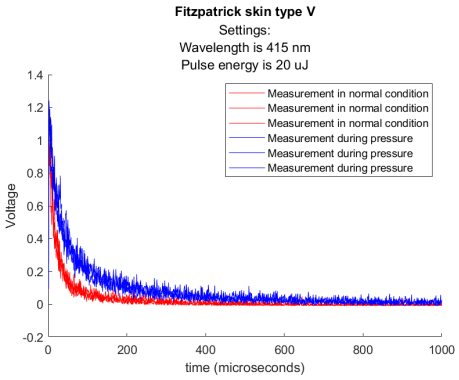

(b) Excitation wavelength: 415 nm; pulse energy: 20 μJ

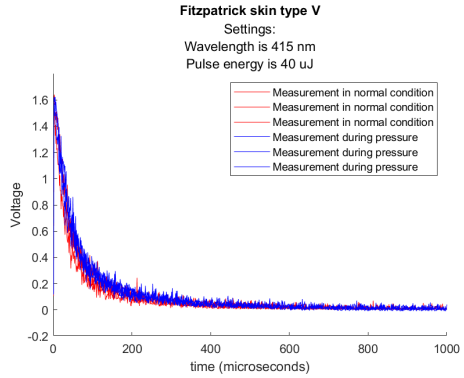

(c) Excitation wavelength: 415 nm; pulse energy: 40 μJ

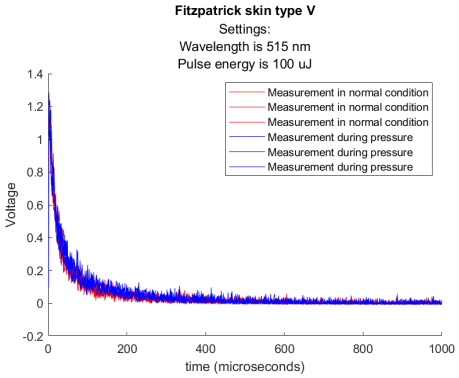

(d) Excitation wavelength: 515 nm; pulse energy: 100 μJ

Figure 43: Measurement in Fitzpatrick skin type V using 415 nm (10, 20 and 40 μJ) and 515 nm (100 μJ).

Combinations of different filters mounted to detector A

Table 3: Available filters

Filter	Qty	Thickness
Band-pass filter 635/20 nm	3x	1.1 mm
Band-pass filter 660/40 nm	3x	1.1 mm
Long-pass filter >610 nm	3x	1.1 mm
Colored glass filter >590 nm	2x	2.0 mm
Absorptive Neutral Density filter	1x	1.5 mm

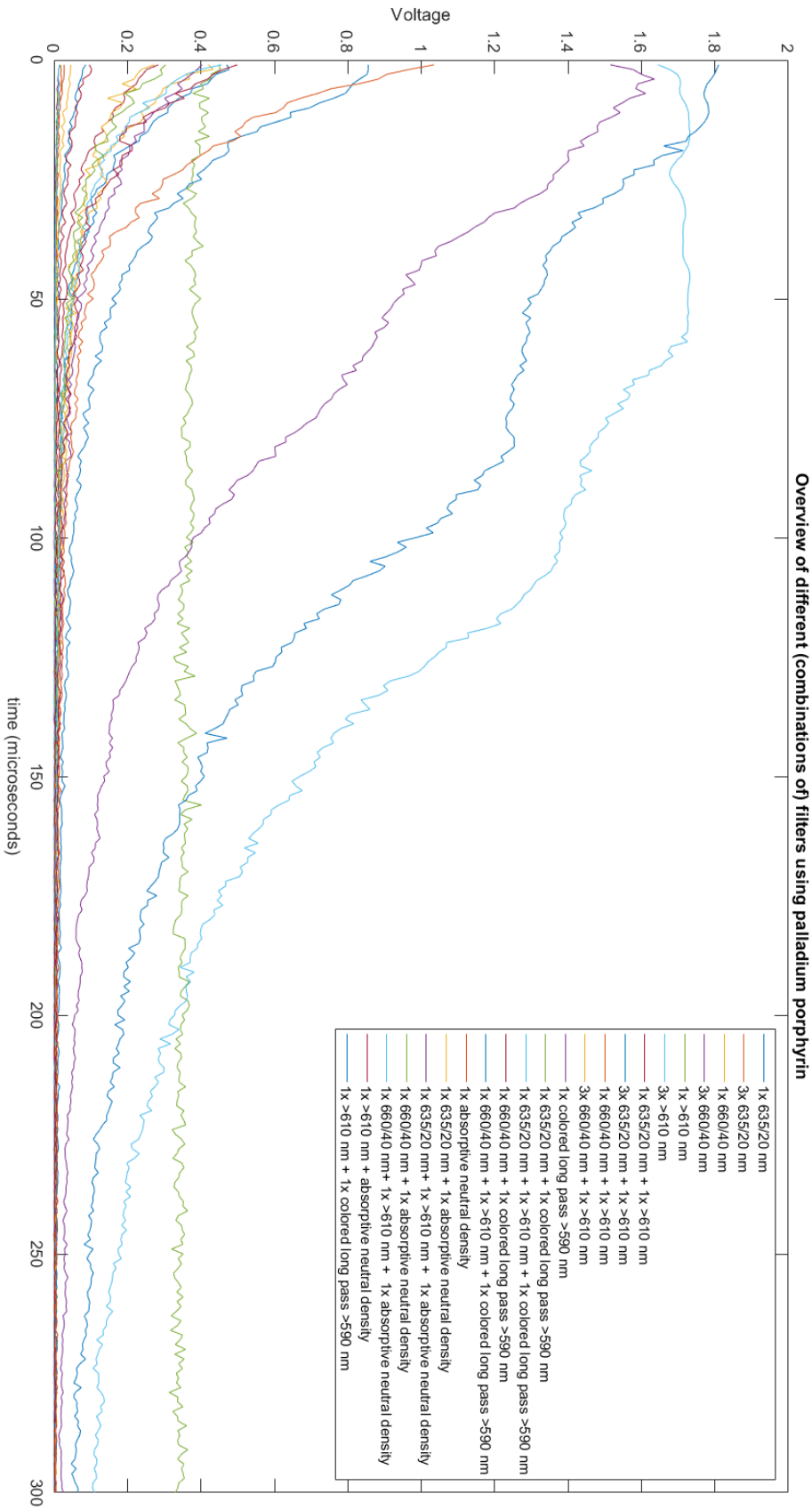

Figure 44: Overview of captured signals using different (combinations of) filters mounted to detector A in a solution of palladium porphyrin.